Received: 25 July 2019 | Revised: 21 December 2019 | Accepted: 22 December 2019

DOI: 10.1002/nbm.4257

SPECIAL ISSUE REVIEW ARTICLE

NMR IN BIOMEDICINE WILEY

Preprocessing, analysis and quantification in single-voxel magnetic resonance spectroscopy: experts' consensus recommendations

Jamie Near[1,2] | Ashley D. Harris[3,4,5] | Christoph Juchem[6] | Roland Kreis[7] | Małgorzata Marjańska[8] | Gülin Öz[8] | Johannes Slotboom[9] | Martin Wilson[10] | Charles Gasparovic[11]

[1]Douglas Mental Health University Institute and Department of Psychiatry, McGill University, Montreal, Canada

[2]McConnell Brain Imaging Centre, Montreal Neurological Institute, Montreal, Canada

[3]Department of Radiology, University of Calgary, Calgary, Canada

[4]Alberta Children's Hospital Research Institute, Calgary, Canada

[5]Hotchkiss Brain Institute, Calgary, Canada

[6]Departments of Biomedical Engineering and Radiology, Columbia University, New York, New York

[7]Departments of Radiology and Biomedical Research, University Bern, Switzerland

[8]Center for Magnetic Resonance Research, Department of Radiology, University of Minnesota, Minneapolis, Minnesota

[9]Support Center for Advanced Neuroimaging (SCAN), Neuroradiology, University Hospital Inselspital, Bern, Switzerland

[10]Centre for Human Brain Health and School of Psychology, University of Birmingham, Birmingham, UK

[11]The Mind Research Network, Albuquerque, New, Mexico

Correspondence
Dr Jamie Near, Room GH-2113, CIC Pavilion, Douglas Mental Health University Institute, Department of Psychiatry, McGill University, Montreal, Canada H4H 1R3.
Email: jamie.near@mcgill.ca

Funding information
Canadian Institutes of Health Research, Grant/Award Numbers: PJT-148751, PJT-165869; Fonds de Recherche du Québec - Santé, Grant/Award Number: FRQ: 0000035275; Natural Sciences and Engineering Research Council of Canada, Grant/Award Numbers: RGPIN-2017-03875, RGPIN-2014-06072;

Once an MRS dataset has been acquired, several important steps must be taken to obtain the desired metabolite concentration measures. First, the data must be preprocessed to prepare them for analysis. Next, the intensity of the metabolite signal(s) of interest must be estimated. Finally, the measured metabolite signal intensities must be converted into scaled concentration units employing a quantitative reference signal to allow meaningful interpretation. In this paper, we review these three main steps in the post-acquisition workflow of a single-voxel MRS experiment (preprocessing, analysis and quantification) and provide recommendations for best practices at each step.

Abbreviations: ^{1}H, proton; ^{13}C, carbon-13; B_0, main magnetic field; B_1, RF field; Cr, creatine; CRMVB, Cramér-Rao minimum variance bound; CSF, cerebrospinal fluid; d_{GM}, water density of grey matter; d_{WM}, water density of white matter; ERETIC, Electric Reference to Access in vivo Concentrations; f_{CSF}, volume fraction of cerebrospinal fluid inside the MRS voxel; $f_{CSF_{H2O}}$, water mole fraction in cerebrospinal fluid; f_{GM}, volume fraction of gray matter inside the MRS voxel; $f_{GM_{H2O}}$, water mole fraction in gray matter; FFT, fast Fourier transform; FID, free induction decay; FQN, fit quality number; FWHM, full width at half maximum; f_{WM}, volume fraction of white matter inside the MRS voxel; $f_{WM_{H2O}}$, water mole fraction in white matter; GM, grey matter; GPC, glycerophosphocholine; $[H_2O]_{molal}$, water concentration in moles of water per kilogram of tissue water = 55.49 moles/kg; $[H_2O]_{molar}$, water concentration in moles of water per liter of tissue water; HERMES, Hadamard encoding and reconstruction of MEGA-edited spectroscopy; MEGA-PRESS, Mescher-Garwood point resolved spectroscopy; $[M]_{GM}/[M]_{WM}$, assumed ratio of grey matter to white matter metabolite concentrations; MM, macromolecules; $[M]_{molal}$, metabolite concentration in moles of metabolite per kilogram of tissue water; $[M]_{molar}$, metabolite concentration in moles of metabolite per liter of tissue water; MRSI, magnetic resonance spectroscopic imaging; NAA, *N*-acetylaspartate; NAAG, *N*-acetylaspartylglutamate; N_M, number of protons contributing to metabolite signal; N_P, number of points in FID/spectrum; N_{pc}, number of phase encoding steps in one phase cycle; N_{RF}, number of RF channels; N_{tra}, number of transients; PCh, phosphocholine; PCr, phosphocreatine; $R_{H2O_{CSF}}$, relaxation scaling factor for water in cerebrospinal fluid; $R_{H2O_{GM}}$, relaxation scaling factor for water in grey matter; $R_{H2O_{WM}}$, relaxation scaling factor for water in white matter; R_M, relaxation scaling factor for tissue metabolite signal; $R_{M_{GM}}$, relaxation scaling factor for metabolite in grey matter; $R_{M_{WM}}$, relaxation scaling factor for metabolite in white matter; S_{H2O}, water signal intensity; $S_{H2O_{obs}}$, observed water signal intensity in the presence of relaxation; S_M, metabolite signal intensity; $S_{M_{obs}}$, observed metabolite signal intensity in the presence of relaxation; SNR, signal-to-noise ratio; SPECIAL, spin echo full intensity acquired localized spectroscopy; T_{acq}, duration of the acquired free induction decay; tCho, total choline; tCr, total creatine; T_E, echo time; T_{E1}, first PRESS echo period; T_{E2}, second PRESS echo period; tNAA, total *N*-acetylaspartate; T_R, repetition time; WM, white matter; $\phi(t)$, phase function of the water FID.

Schweizerischer Nationalfonds zur Förderung der Wissenschaftlichen Forschung, Grant/Award Number: 320030-175984; Institutional Centre Cores for Advanced Neuroimaging award, Grant/Award Number: P30 NS076408; National Institute of Biomedical Imaging and Bioengineering, Grant/Award Number: P41 EB015894; National Institute of Neurological Disorders and Stroke, Grant/Award Number: R01 NS080816

KEYWORDS

analysis, MRS, preprocessing, processing, quantification, quantitation, water referencing

1 | INTRODUCTION

The goal of an in vivo MRS experiment is to estimate the relative or absolute concentrations of tissue metabolites within a specific anatomical region of interest. Once the time domain MRS data have been acquired, several steps are needed in order to obtain meaningful and reliable concentration estimates. First, a series of *preprocessing* steps should be applied to prepare the spectrum for analysis. Next, *analysis* of the processed dataset is performed, often by peak fitting, to estimate the metabolite signal intensities. Finally, the unitless signal intensity measures are converted into scaled concentration estimates, a process we refer to here as *quantification*, to enable meaningful interpretation and comparisons of tissue metabolite levels between subjects and groups, regardless of the site of acquisition or other measurement conditions. Each of these three steps is critically important; errors in any of them can reduce the reliability of, or completely invalidate, the obtained metabolite concentration measures.

In this article, we focus on these three important steps in the workflow of single-voxel proton (^{1}H-)MRS following data acquisition: *preprocessing*, *spectral analysis* and *quantification*. We describe some of the most important and commonly used approaches in each step, and provide recommendations for best practices (see tables for all recommendations). Finally, we list common pitfalls in the post-acquisition workflow and suggest ways to avoid them. Though the emphasis in this article is on single-voxel ^{1}H-MRS, with attention to the challenges of its application in the brain, many of the general principles of the post-acquisition workflow apply to MRS data obtained from other nuclei, other regions of the anatomy and magnetic resonance spectroscopic imaging (MRSI) data. For more information regarding MRSI specific processing and analysis methods, the reader is referred to the article on MRSI in this special issue by Maudsley.[1]

2 | PREPROCESSING

Preprocessing of MRS data, sometimes also simply called "processing", describes any operation, or series of operations, that is applied to the acquired raw MRS data (free induction decays, FIDs) to prepare them for analysis. There are three main reasons for preprocessing in MRS. First, MRS data are unavoidably degraded by experimental imperfections (e.g., eddy currents, scanner drift, subject motion). Since spectral fitting models generally do not take all of these imperfections into account, some preprocessing operations are needed to remove the imperfections, to the extent possible, in advance. Second, raw data are almost always multi-dimensional, with multiple signal averages acquired by multiple coil channels from parallel receive array coils. Thus, some preprocessing is needed to combine these signals and reduce the data into a (usually) one-dimensional spectrum that can be analyzed. Finally, some other preprocessing operations, such as Fourier transformation, phasing, apodization and zero-filling, are not strictly related to data quality, but can be used to aid in visual interpretation or peak fitting performance.

Note that several of the preprocessing routines described below require access to the individual averages or transients, stored independently for each receiver channel. Accordingly, we strongly recommend the use of data formats in which the individual transients and individual receiver channels are preserved. At present, each MRI vendor has its own unique data formats, and each format differs in regard to which dimensions are preserved and which have been collapsed (implying some "online" preprocessing, see Table 1). The lack of cross-vendor standardization in terms of MRS data formats and online preprocessing strategies can be a source of confusion, and represents a major unmet need in the MRS community.[2]

2.1 | Preprocessing operations to remove/correct spectral imperfections

2.1.1 | Correction of eddy current effects

Rapid gradient switching gives rise to unwanted short-lived fluctuations of the B_0 field, called eddy current effects, which can persist for hundreds of milliseconds after a gradient switching event. If the acquisition window occurs close to the end of a gradient pulse, a multi-exponential

TABLE 1 Scanner vendor data formats

Vendor	Data format	File naming convention	Dimensionality (default)	Comments
GE	p-file	P01234.7	$N_p \times N_{tra}/N_{pc}$	-by default, RF coil channels pre-combined online; and groups of N_{pc} phase cycle steps pre-combined online. The resulting number of separately stored transients is N_{tra}/N_{pc}. -however, the p-file can be customized to preserve or combine any/all dimensions. -both water and metabolite data may be stored within the same series.
Philips	data/list	filename.data filename.list	$N_p \times N_{tra}$	-water and metabolite data are normally stored in separate files, but some pulse sequences may store both within the same series. -depending on settings, water unsuppressed transients may be interleaved within groups of water suppressed transients, and frequency drift correction may have been applied. -two files for each acquisition: .data file contains the acquired signal data; .list file contains header info.
	sdat/spar	filename.sdat filename.spar	$N_p \times N_{tra}/N_{pc}$	-separate files for water and metabolite data. -two files for each acquisition: .sdat file contains the acquired signal data; .spar file contains header info.
Siemens	Twix	filename.dat	$N_p \times N_{RF} \times N_{tra}$	-all dimensions (RF channels, transients) are preserved without modification. - water and metabolite data are normally stored in separate files, but some pulse sequences may store both within the same series.
	rda	filename.rda	N_p	-by default, all dimensions (except time/spectral dimension) are pre-combined online. -however, .rda files can be customized to preserve or combine any/all dimensions. - water and metabolite data are normally stored in separate files, but some pulse sequences may store both within the same series.
	.ima	filename.ima	N_p	-by default all dimensions (except time/spectral dimension) are pre-combined online. -however, .ima files can be customized to preserve or combine any/all dimensions. In this case, each individual transient is stored in a separate .ima file. - water and metabolite data are normally stored in separate files, but some pulse sequences may store both within the same series.
Bruker	fid file	fid	N_p	-all dimensions (except time/spectral dimension) are pre-combined online. -separate files for water and metabolite data.
	fid.raw file	fid.raw (up to PV 5)	$N_p \times N_{tra}$	-RF channels are pre-combined online. -all transients are preserved without modification. -separate files for water and metabolite data.
	job0 file	Rawdata.job0 (PV 6 and later)	$N_p \times N_{tra}$	-RF channels are pre-combined online.

(Continues)

TABLE 1 (Continued)

Vendor	Data format	File naming convention	Dimensionality (default)	Comments
				-all transients are preserved without modification. -separate files for water and metabolite data.
Varian/Agilent	fid file	fid	$N_p \times N_{RF} \times N_{tra}$	-full flexibility to preserve or collapse all dimensions. -separate files for water and metabolite data.
DICOM (any vendor)	DICOM	Various, e.g., filename.dcm	N_p	-by default, all dimensions are collapsed. -however, dicom files can be customized to preserve or combine any/all dimensions. In this case, each individual transient may be stored in a separate dicom file. -separate files for water and metabolite data.

N_p, number of points in the FID.
N_{RF}, number of RF channels.
N_{tra}, number of transients.
N_{pc}, number of phase encoding steps in one phase cycle.

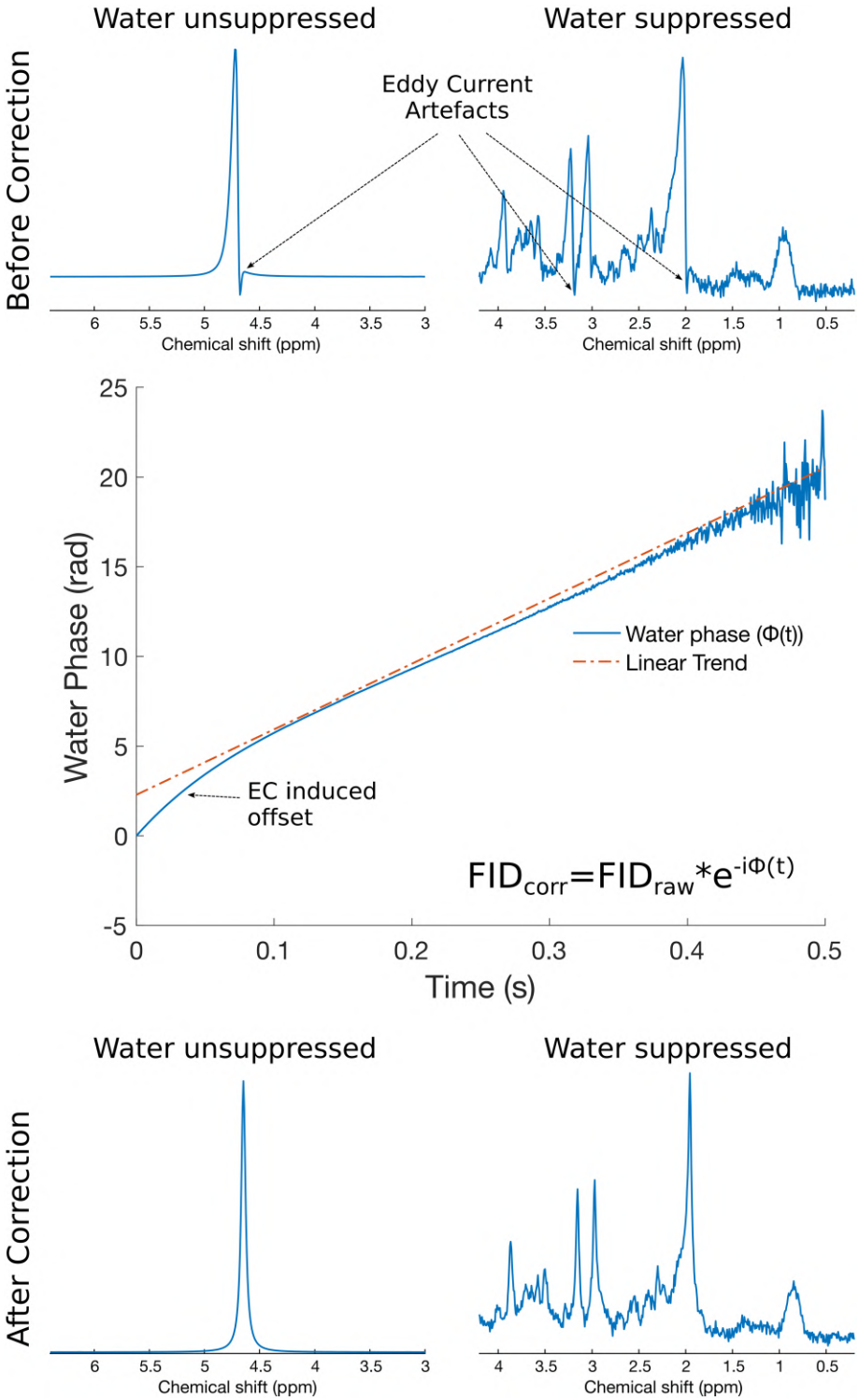

FIGURE 1 Eddy current correction in synthetic 3 T human brain PRESS spectra with T_E = 30 ms. in the top panel, water reference (left) and water-suppressed (right) spectra with eddy current artefacts are shown. The central panel shows the phase evolution of the water reference FID before eddy current correction. Any deviation from linearity in this phase function is the result of the eddy current effect. The bottom panel shows the same water reference (left) and water-suppressed (right) spectra following eddy current correction

decaying B_0-field component may exist during the early part of the acquisition window, giving rise to a time dependence in the resonance frequencies of the acquired FID. This unwanted effect distorts spectral line shapes and can severely impact the robustness of further spectral analysis.

The most common method of dealing with this issue involves collecting an unsuppressed water spectrum, centered on the water resonance, using identical gradient strengths and timings as in the water-suppressed dataset.[3] Any time dependence in the frequency of the water signal will be observed as a non-linearity in the phase of the FID signal. Since this phase function essentially describes the time dependence of the field offset observed in both water-suppressed and water-unsuppressed scans, the correction involves simply subtracting this phase function from both the water-suppressed and water-unsuppressed FID signals. This simple approach is remarkably effective in most cases, and results in FID signals that are essentially free of residual eddy current effects. Related methods exist for correcting eddy current effects while simultaneously restoring

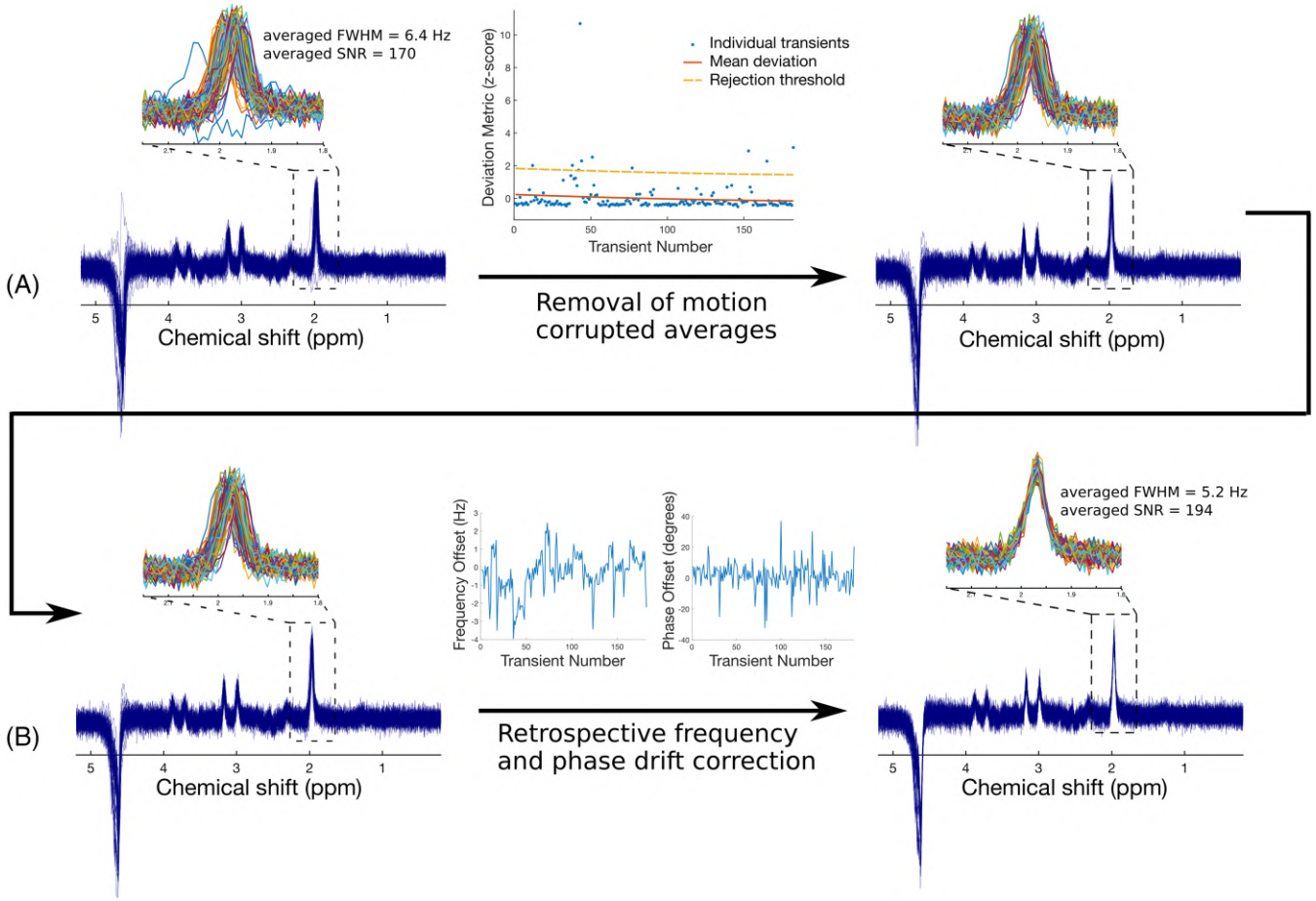

FIGURE 2 Removal of corrupted transients and retrospective frequency and phase drift correction from a 3 T human brain PRESS acquisition with T_E = 270 ms. A, Removal of motion-corrupted transients. Corrupted transients stand out as noticeably different from the others, and are effectively removed using an unsupervised outlier removal procedure (see reference 15). B, subsequent retrospective frequency and phase drift correction. Following drift correction using spectral registration, the individual transients have improved coherence and can now be averaged. These processing steps yield a marked improvement in both the full-width at half-maximum (FWHM) and SNR of the final averaged spectrum

purely Lorentzian line shapes by applying both phase and amplitude scaling to the acquired FID.[4,5] An eddy current correction is illustrated in Figure 1.

2.1.2 | Motion correction

Subject motion has pronounced effects on spectral quality. Despite all efforts to control subject motion, a small amount of motion is practically inevitable in the timeframe of an MRS scan. One practical way to test for gross motion is to acquire a quick localizer image immediately before and after the MRS scan and compare the position of the anatomy of interest between those two scans. Better yet, the collection of rapid navigator images between each repetition,[6-11] or optical tracking,[12,13] can be used to precisely monitor subject motion, and even update the acquisition volume in real time to compensate. Although highly promising, these prospective motion correction strategies for ^{1}H-MRS are not yet in mainstream use, and thus retrospective correction methods are commonly employed.

Very small amounts of motion, for example due to normal physiological motion (breathing, cardiac pulsation, swallowing) or small bulk movements of less than a few millimeters, have a minor effect on spectral quality and are therefore relatively benign in most cases. These minute motions result in small changes in the frequency and phase of the individual transients, which can easily be corrected by a retrospective frequency and phase drift correction (see below). In the case of large amounts of motion such as gross motion of the head or limbs, much larger spectral distortions are observed.[14] Moreover, severe gross motion can lead to unwanted sampling of tissue outside the region of interest. In this case, it may be necessary to either remove the transients that are most severely affected by motion,[15] or to discard the dataset altogether. To assess motion severity in a quantitative and unbiased way, signal reliability tests have been proposed.[16] An example of the removal of motion-corrupted transients is illustrated in Figure 2A.

2.1.3 | Retrospective removal of frequency and phase drifts

The main magnetic field of an MRI scanner, B_0, is subject to subtle temporal drift (often called scanner drift), due to heating and cooling of the ferromagnetic passive shim elements, which are in thermal contact with the gradient coils.[17] As a result, frequency drifts are observed during the course of most MRS experiments. The magnitude of these drifts can vary greatly from scanner to scanner and is also affected by use of gradient-intensive pulse sequences before the MRS scan, but normally ranges between 1 and 10 Hz of total drift during the course of a typical MRS acquisition (i.e., 2–10 min). Moreover, as mentioned above, physiological motion or small bulk motion during the MRS scan leads to additional frequency and phase offsets, independent of scanner drift. If not corrected, these frequency and phase drifts will lead to broadening of spectral peaks, reduction in signal-to-noise ratio (SNR) and line shape distortion.

Several methods exist for retrospective correction of frequency and phase drifts. Some involve tracking the frequency and phase of the residual water peak to estimate and correct the frequency and phase drifts,[11,18-21] while others make use of separately acquired navigator echoes.[22] If a residual water peak or navigator echoes are not available for frequency and phase estimation, individual metabolite peaks can also be used.[23] More recently, methods such as spectral registration,[24] RATS[25] or other variants[26,27] have been proposed, and involve alignment of each transient, in either the frequency domain or the time domain, to a reference spectrum for estimation and correction of the frequency and phase offsets. The advantage of these latter methods is that they make use of the full spectrum to perform the correction, and do not rely on the presence of any one particular resonance. Most algorithms optimize the frequency and phase in a single step, rather than sequentially. An example of retrospective frequency and phase drift correction is illustrated in Figure 2B. In some cases, an online frequency drift correction may be employed by the scanner software. While the use of such online corrections is recommended, it may be advantageous to apply an additional retrospective drift correction offline, since online corrections may correct frequency, but not phase drifts.

Frequency and phase drift correction methods that rely on internal signals for alignment will inevitably fail if the SNR of the individual transients is low (for example if the voxel is very small). In such cases, one can average successive groups of four to eight transients to improve SNR, and then apply a drift correction to the resulting series. Alternatively, a method called metabolite cycling[28-31] has been proposed, in which the water peak is not suppressed, but the magnetization of the metabolites is inverted on every other acquisition. In this way, the high-SNR water peak can be used for drift correction, even if the metabolite SNR is low. When the averages are combined the water peak essentially vanishes due to its alternating phase from shot to shot.

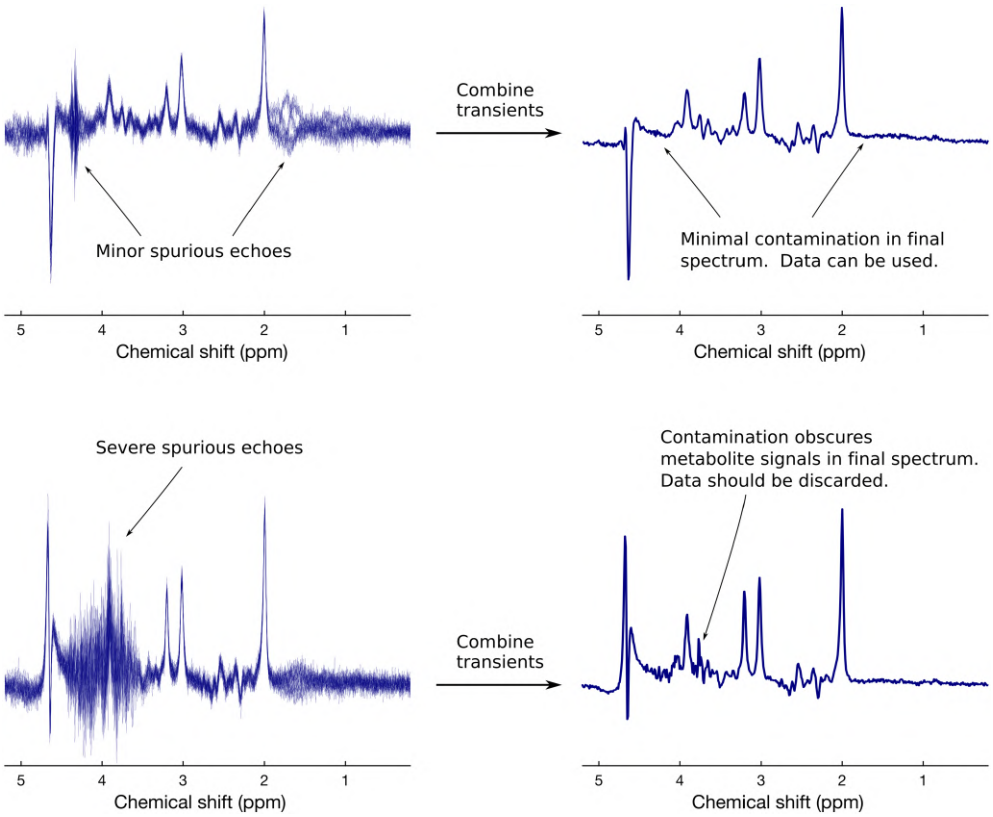

FIGURE 3 Examples of spurious echoes in 3 T human brain MRS data (T_E = 68 ms). In the top panel, minor spurious echoes are observed in the individual transients around 1.8 ppm and 4.3 ppm. However, following averaging of the phase-cycled scans, these are effectively removed, so that this spectrum can be safely analyzed. In the bottom panel, severe spurious echoes are observed in the individual transients between 3.5 and 4.6 ppm. Even after combining these phase-cycled averages, visible contamination remains (e.g., overall jagged character of the spectrum between 3.6 and 4.4 ppm, distortion of the glutamate-H2 doublet at 3.75 ppm and distortion of the *myo*-inositol peak at 4.1 ppm), and this spectrum should therefore be discarded

TABLE 2 Recommendations for preprocessing operations to remove/correct spectral imperfections

Name of operation	Recommendation
Eddy current correction	- an eddy current correction should be applied routinely during the preprocessing of any in vivo MRS dataset. - for accurate eddy current estimation, the unsuppressed water scan must be collected from the same voxel location and using exactly the same gradient scheme as the water-suppressed data (e.g., turn only water suppression RF pulses off for unsuppressed water acquisition). - some analysis software packages (LCModel,[46] Tarquin,[47] FiTAID[48]) perform an eddy current correction at the analysis stage, obviating the need to perform this step in advance.
Motion correction	- for small amounts of motion, correct the resulting frequency and phase jitter using a frequency and phase drift correction (see below). - more severe bulk motion is indicated by individual transients that stand out as significantly different from the rest. Identify these "corrupted" transients either by visual inspection or by unsupervised outlier detection, and remove them prior to analysis. - if more than ~30% of the acquired transients are corrupted by motion, we recommend discarding that particular dataset since (a) the likelihood of significant unwanted sampling of tissue outside the region of interest is high, and (b) the continued removal of transients has a detrimental effect on the final SNR.
Frequency and phase drift correction	- frequency and phase drift correction should be applied routinely for in vivo MRS, provided that there is enough SNR in the individual (or a few summed) transients to achieve robust frequency and phase estimation. - there are many effective methods for retrospective frequency and phase drift correction. We recommend methods that make use of the full spectrum (unless a weakly suppressed water peak is used for alignment). -where available, the use of vendor-provided online drift corrections is recommended, provided that their performance has been well validated; but offline retrospective drift correction is still recommended.
Alignment of subtraction sub-spectra	- subtraction-based MRS techniques should always be coupled with an appropriate alignment procedure to align sub-spectra prior to subtraction. The choice of alignment procedure depends on the acquisition method. - in *J*-difference edited MRS, retrospective alignment of subtraction sub-spectra does not restore drift-induced reductions in editing efficiency.
Nuisance peak removal	- it is *always* preferable to remove nuisance signals at the level of the acquisition, rather than via preprocessing. - if necessary, large water and lipid signals can either be removed prior to analysis, or accounted for in the analysis model. Alternatively, one can adjust the frequency range over which spectral analysis is performed in order to avoid nuisance signals. - spurious echoes should be identified by visual inspection. - since processing methods to remove spurious echoes are not widely available, we recommend that spectra contaminated by large spurious echoes should be discarded from further analysis, particularly if the spurious echoes are obscuring the metabolite peaks of interest.

2.1.4 | Alignment and subtraction of sub-spectra

^{1}H-MRS pulse sequences involving subtraction are increasingly common. Some examples include *J*-difference editing sequences such as MEGA-PRESS (Mescher-Garwood point resolved spectroscopy)[32] and HERMES (Hadamard encoding and reconstruction of MEGA-edited spectroscopy)[33]; or the SPECIAL (spin echo full intensity acquired localized spectroscopy) sequence,[34] which uses subtraction to achieve localization. If the sub-spectra in these acquisitions are not properly aligned prior to subtraction, the resulting difference spectrum may be corrupted by unwanted subtraction artefacts that can impact quantification.

Alignment of subtraction sub-spectra can be performed using the same techniques as are used for removal of frequency and phase drift in conventional spectra (e.g., spectral registration etc).[35,36] However, if subtraction sub-spectra are vastly different in appearance, conventional alignment procedures may not perform well, and dedicated routines may be required for optimal alignment. Dedicated alignment algorithms have previously been proposed for MEGA-PRESS,[37,38] HERMES[39] and SPECIAL.[15]

Substantial frequency drift during *J*-difference edited acquisitions results in reduced editing efficiency, due to offsets in the frequency of the highly selective editing pulses. This effect is not corrected by retrospective alignment of the subtraction sub-spectra. Instead, drift-related reductions in editing efficiency must be addressed at the level of the acquisition (using real time frequency updating[10]), or in the analysis (by accounting for drift-related editing efficiency losses in the basis set[40]). For more information on this topic, the reader is referred to the article on spectral editing in this special issue by Choi.[41]

2.1.5 | Nuisance peak removal (residual water, lipids, spurious echoes)

In vivo ^{1}H-MRS acquisitions are specifically designed to suppress nuisance signals such as water and outer volume signal. However, perfect suppression is challenging, as the signals to be suppressed are usually orders of magnitude larger than the signals of interest. As a result, noticeable contamination of spectra is a relatively common occurrence, especially in challenging brain regions (regions very close to the scalp, or regions with

poor B_0 homogeneity), and minimizing signal contamination is an important aspect of data preprocessing. Note that even though nuisance signals can sometimes be addressed via processing strategies, it is *always* preferable to remove these contaminating signals at the level of the acquisition.

Poor water suppression can be handled in two ways. Residual water signal can be removed prior to spectral analysis by fitting the peak to a line shape function—usually either Gaussian, Lorentzian or Voigt (combination of Gaussian and Lorentzian)—or to a series of line shape components via singular value decomposition, and then subtracting the resulting fit from the spectrum.[42,43] Another approach is to not remove the water peak, but to perform analysis using a fitting model that incorporates a water peak (or the sloping baseline that results from the residual water peak). Lipid contamination, like poor water suppression, can impact spectral quantification and can be dealt with in a similar manner, with the main difference being that contaminating lipid peaks are generally much broader than residual water peaks and often overlap with metabolites of interest, often making lipid contamination more difficult to correct.

Spurious echoes are another commonly observed nuisance signal in in vivo ^{1}H-MRS. These are typically caused by unwanted coherence pathways and often originate from tissues outside the region of interest. The issue of unspoiled coherences is best dealt with by modifications to the acquisition, such as changing the timing or amplitudes of the spoiler gradients, improving B_0 homogeneity or improving the phase cycling scheme.[14,44] A few preprocessing approaches have been proposed to identify and remove spurious echoes, based on filtering or deep learning,[45] but these methods are still relatively new and may require further development before being deployed widely. Spurious echoes may occur near the end of an FID, in which case apodization can be used to greatly reduce their appearance; but users should analyze the resulting data with caution, since apodization is not recommended before spectral analysis (see section 2.3.3). An example of commonly observed spurious echoes is shown in Figure 3.

Recommendations for the preprocessing operations to remove/correct spectral imperfections are listed in Table 2.

2.2 | Preprocessing operations to reduce dimensionality

2.2.1 | RF coil combination

Most modern MRI systems are equipped with highly parallel RF receiver arrays, sometimes with as many as 64 or even 128 elements in close proximity to the head. Each of the receiver elements will detect different signal and noise amplitudes as well as a different signal phase offset that will depend on the voxel location and head position relative to the coil element. Combining the signals from the various coil elements should be done in a way that maximizes the SNR of the resulting spectrum. In all cases, this requires (1) adjusting the phase of each channel so that all elements are phase coherent and (2) applying an amplitude weighting to each channel for optimal SNR combination. The RF channels with the strongest signals are given the highest weighting, while the RF channels with the weakest signals are given the lowest weighting.[49,50] The amplitude, phase and noise terms necessary for coil combination can generally be determined from the high-SNR unsuppressed water data.

2.2.2 | Signal averaging

Signal averaging is the process of taking the average of the acquired transients (the sum of all transients divided by the number of transients) to produce a resultant spectrum with increased SNR. The convention of averaging transients ensures that the signal remains constant, while noise is

TABLE 3 Recommendations for preprocessing operations to reduce dimensionality

Name of operation	Recommendation
RF coil combination	- most vendors provide a data output option in which an acceptable RF coil combination has already been performed. - however, if the raw data are provided with coils uncombined, the user must perform coil combination. - coil combination should include appropriate complex weights (phase and amplitude). - complex weights should be determined using an unsuppressed water scan. - the amplitude weighting should be generally determined by signal/noise^2 as per Hall et al.[49] although more sophisticated approaches may yield improved results for certain coil designs and voxel locations.
Signal averaging	- we recommend combining transients using the arithmetic mean (the sum of all transients divided by the number of transients). Although less robust to instabilities across transients than the median, we suggest dealing with these instabilities through removal of motion-corrupted averages and frequency/phase drift correction prior to averaging. -if motion-corrupted transients have been removed, divide only by the number of transients that were retained. - avoid combining averages using the simple sum of the acquired transients (i.e., the sum should always be divided by the number of transients). - likewise, subtraction operations used in difference spectroscopy should also be treated as an averaging operation; i.e., when subtracting sub-spectra of a MEGA-PRESS difference editing experiment or a SPECIAL localization experiment, the difference spectrum should always be divided by 2 (the number of transients involved in the subtraction) following subtraction.

reduced (subjectively); thus, subsequent quantification of signal intensity in "averaged" spectra requires no consideration of the number of transients. Despite the fact that the arithmetic mean is by far the most common approach for combining transients, some authors have proposed taking the median of the acquired transients as an alternative approach, suggesting that the median is more robust against temporal instabilities in the signal.[16]

Recommendations for preprocessing operations to reduce dimensionality are listed in Table 3.

2.3 | Other preprocessing operations

2.3.1 | Fourier transformation

Conversion of the discrete time-domain FID signal into a spectrum is performed using a discrete Fourier transformation such as fast Fourier transform (FFT). Most software programming languages offer a built-in implementation of the FFT, and all MRS software packages will perform the Fourier transformation by default. To convert from the spectral domain back to the time domain, the discrete inverse Fourier transform should be used.

2.3.2 | Phasing

Whereas MRI signal intensities are generally displayed as the magnitude of the complex signal intensity at each voxel, it is most common in MRS to display the real part of the complex signal, to avoid unwanted spectral broadening. As a result, the spectral appearance is strongly influenced by the phase of the complex spectral points, which depends on many factors, including cable lengths, receiver phase, RF pulse phase, voxel position, pulse sequence timing etc. In most cases, an "in-phase" spectrum is one in which the prominent singlet peaks display an absorption line shape, meaning that they are upright and symmetric (assuming minimal eddy current artefacts). Some spectral analyses may require that the spectrum first be "in phase", but many common analysis packages either perform an automatic phasing step prior to fitting, or include phase as a fitting parameter, so it is often not necessary for the user to perform this step in advance.

Phase correction involves either adding a constant phase to each point in the spectrum (zero-order phasing), or adding a linear phase shift as a function of frequency (first-order phasing), until the spectrum appears "in phase." Manual zero- and first-order phasing is a common approach; however, identifying a correctly phased spectrum takes practice and can be somewhat subjective. Therefore, automated phasing routines[51-53] can be useful.

2.3.3 | Apodization

Apodization is a procedure aimed at attenuating the noise in an MR spectrum, while preserving the signals of interest. Conveniently, the signals of interest are strongest at the beginning of the FID signal in the time domain, whereas the later part of the FID is mostly noise. Thus, by applying an

TABLE 4 Expert recommendations for other processing operations

Name of operation	Recommendation
Fourier transformation	- an implementation of a discrete Fourier transformation, such as the FFT, should be used to convert the time-domain FID signal into a spectrum. - conversion from the spectral domain back to the time domain should be performed using the inverse discrete Fourier transform.
Phasing	- some common data analysis packages perform an automated phasing step prior to fitting, so it is often not necessary to perform a phasing step in advance of spectral analysis. - phasing should generally be performed prior to displaying or inspecting a spectrum to enable easy visual interpretation. - both manual and automated phasing routines are equally acceptable, but visual verification of automatic phasing results is recommended.
Apodization	- apodization can be useful for visualization purposes. - not recommended to apodize data prior to spectral analysis—this can invalidate statistical assumptions associated with the fitting model.
Zero-filling	- zero-filling before spectral analysis is not recommended. - may be helpful prior to some other processing routines such as peak fitting for linewidth estimation or center frequency estimation. - use of zero-filling is recommended if increased digital resolution is required.

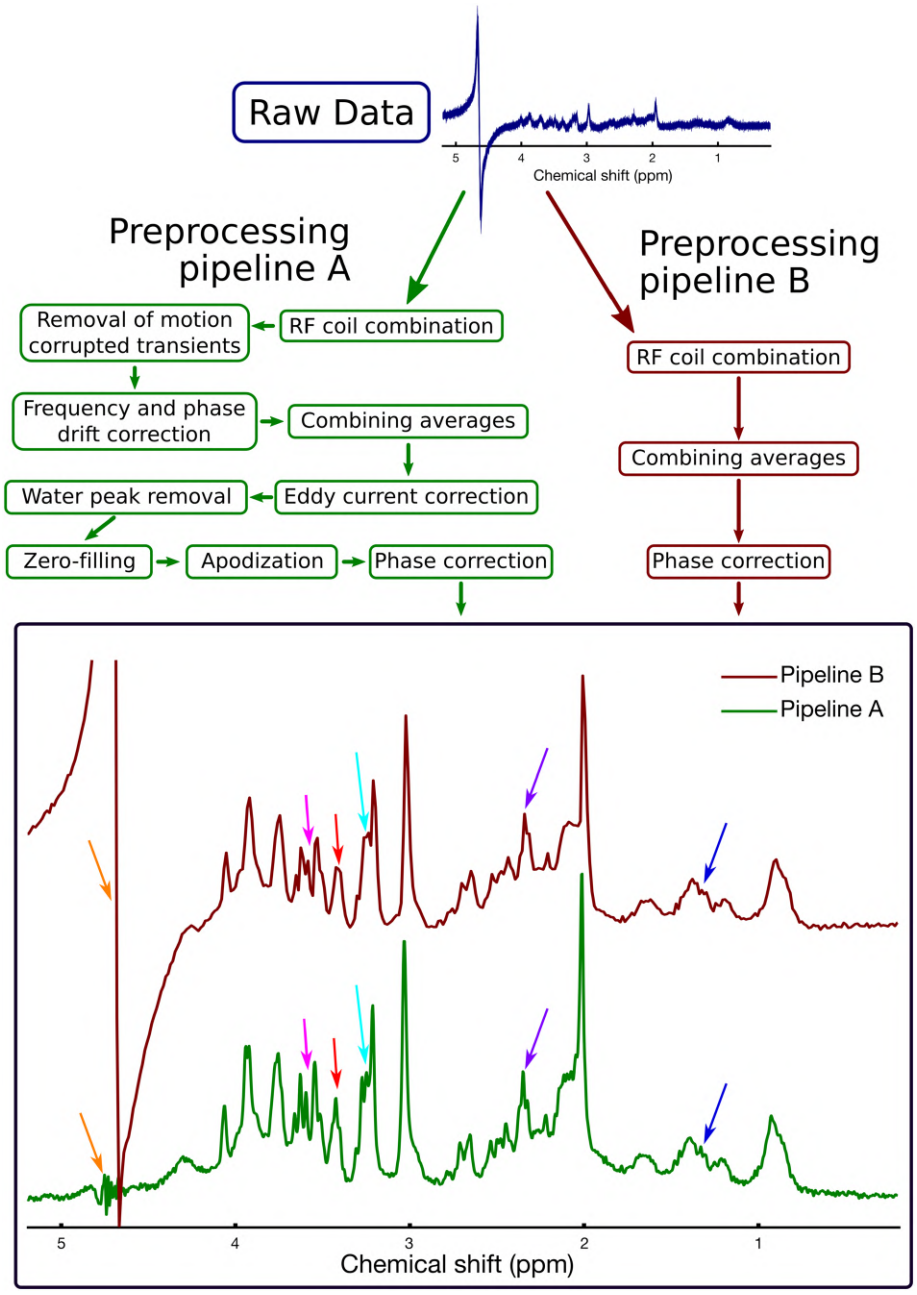

FIGURE 4 Illustration of two example processing pipelines, applied to the same raw data. The dataset was obtained from a rat brain using the PRESS sequence at 7 T with T_E = 11 ms. Processing pipeline B (dark red boxes, right-hand side) includes only basic steps to combine the coils and transients (similar to the standard processing pipeline provided by clinical scanner vendors). Processing pipeline A (green boxes, left-hand side) involves additional steps to remove motion-corrupted averages, to retrospectively correct frequency and phase drift, and to remove eddy current artefacts. Pipeline A resulted in several noticeable improvements in spectral quality, including reduced water contamination (orange arrows), and improved visual definition of most spectral peaks, including lactate (1.3 ppm, dark blue arrows), glutamate-H4 (2.3 ppm, purple arrows), tCho (3.2 ppm, light blue arrows), taurine (3.4 ppm, red arrows) and *myo*-inositol (3.5 ppm, pink arrows). These improvements highlight the importance of using an appropriate processing pipeline. Note that, as stated in the recommendation tables, zero-filling and apodization may be used to improve the visual appearance of the spectrum, but should not be performed prior to spectral analysis

apodization function in the time domain which gives a higher weight to the early timepoints and a lower weight to the later timepoints, the desired effect is achieved. Apodization also minimizes truncation artefacts that occur due to incomplete FID decay during the acquisition window. Common apodization functions include an exponential or Gaussian decay. Although apodization reduces noise and generally improves SNR, it also has some unwanted consequences, such as broadening/distortion of spectral line shapes. As a result, apodization can have significant impact on analysis and quantification results, and is generally recommended for visual display purposes only.

2.3.4 | Zero-filling

The digital resolution of an MR spectrum (frequency spacing between adjacent spectral samples) is given by $1/T_{acq}$, where T_{acq} is the duration of the acquired FID signal. Thus, if the acquisition duration is especially short, the resulting spectrum may have limited digital resolution. This problem can be addressed by zero-filling (sometimes called zero-padding), whereby a train of zeros is added to the end of the FID signal. This artificially lengthens the FID (increases the value of T_{acq}) and therefore increases the digital resolution of the spectrum, without adding any additional noise. However, it is important to realize that this operation amounts to an interpolation operation in the frequency domain and does not improve

the actual resolution of the spectral peaks. For this reason, zero-filling before spectral analysis is not recommended. Nonetheless, zero-filling can be useful for visualization and display purposes, or for improving the stability of certain other operations such as evaluation of peak height, peak frequency or linewidth.

Recommendations for other preprocessing operations are listed in Table 4.

Figure 4 shows two preprocessing pipelines: one that includes only basic steps to combine the coils and transients (similar to the standard preprocessing pipelines provided by clinical scanner vendors), and a second involving additional steps to remove motion-corrupted averages, to retrospectively correct frequency and phase drift, and to remove eddy current artefacts. When the same dataset is processed separately through these two pipelines, the resulting differences in spectral quality are apparent, highlighting the importance of removing motion-corrupted scans and correcting frequency and phase drift.

Following preprocessing, the user must judge whether the quality of the final processed spectrum is adequate for meaningful analysis and quantification. This judgement should incorporate objective measures of spectral quality (linewidth and SNR), but may ultimately require consideration of factors that are difficult to quantify objectively, such as the presence of artefacts or nuisance signals. Recent advances in machine learning techniques have made it possible to objectively assess all of the above aspects of spectral quality in an automated fashion,[54-56] thereby avoiding any potential user bias associated with visual inspection by human raters, but these approaches do not yet enjoy mainstream use.

3 | ANALYSIS

After preprocessing, the spectrum is ready for the next stage: spectral analysis. The goal of spectral analysis is to estimate the spectral peak areas (or equivalently, time-domain signal amplitudes) of the various metabolites of interest in the spectrum, as well as that of some reference signal. At this stage, the units of measurement are not important: only the relative raw signal intensities are needed. These will be converted to meaningful concentration units in the next stage (quantification). In this section, we will briefly summarize the process of spectral analysis and provide some basic recommendations.

The three most common ways of estimating MRS peak areas are (1) linear combination model fitting, (2) peak fitting and (3) peak integration.

3.1 | Linear combination model fitting

In linear combination model fitting, each metabolite's contribution to the overall spectrum is modelled as a single response function called a "basis spectrum." The basis spectrum describes an individual metabolite's full spectral contribution, and can be obtained either by phantom experiment[46]

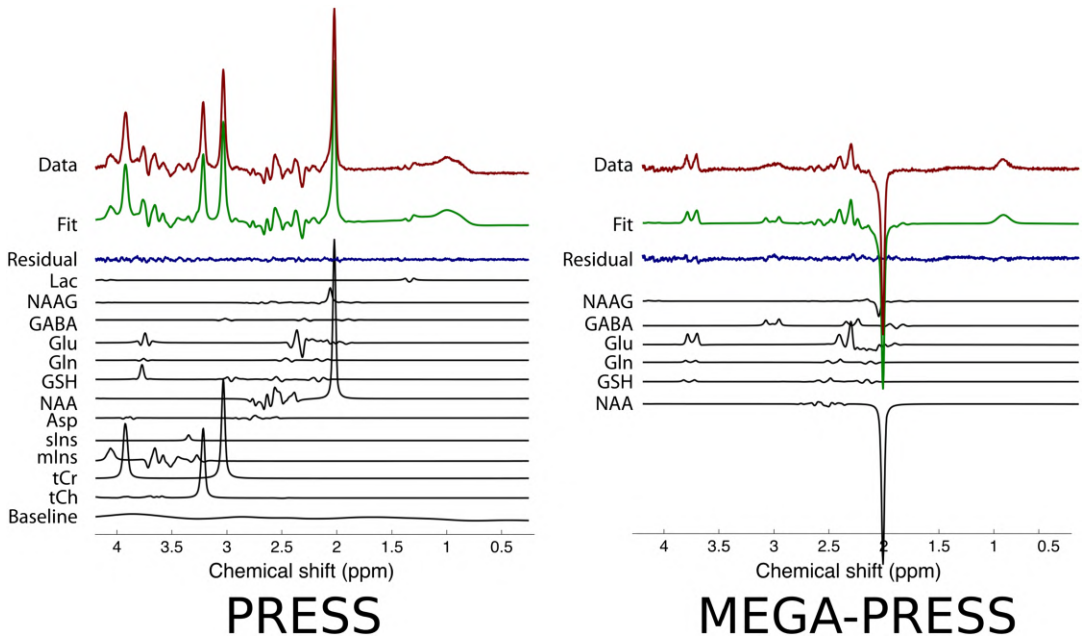

FIGURE 5 Two examples of linear combination model fitting are shown. In both cases the acquired data are displayed at the top in dark red, the overall fit is displayed second from the top in green, and the fit residual is displayed third from the top in dark blue. Below the fit residual, the individual metabolite fit components are displayed in black. The example on the left is from a 3 T human brain PRESS spectrum with T_E = 68 ms. The example on the right is from a 3 T human brain MEGA-PRESS difference edited spectrum with T_E = 68 ms. Note the small peaks around 3.0 ppm in the MEGA-PRESS fit residual, indicating imperfect modelling of the GABA signal due to MM contamination

or by numerical simulation.[15,57-61] A major advantage of using basis spectra over individual peak components is that it greatly reduces the total number of model functions required to fully model the spectrum, resulting in fewer parameters to fit, and a corresponding reduction in the Cramér-Rao minimum variance bound (CRMVB) estimates (the most commonly used measure of the uncertainty of the model fit parameter estimates). Moreover, since basis spectra are generated directly from experiment or simulation, they are physically realistic, and can be highly accurate. Once the full set of metabolite basis spectra (the basis set) is produced, a constrained non-linear least-squares analysis can be used to fit a linear combination of the basis spectra to the acquired MR spectrum by adjusting their individual amplitudes and frequencies. Additional global terms such as spectral phase and linewidth are normally included to improve the fit, thus necessitating the non-linear least-squares approach. The relative amplitudes (or weights) of the various metabolite basis spectra in the best fit correspond to the estimated relative signal intensities. The fit residual—the difference between the fit and the data—provides an indicator of the goodness of fit, or the presence of unmodelled peaks in the spectrum. Quantitatively, this can be expressed using the fit quality number (FQN), which is the ratio of the variance in the fit residual divided by the variance in the pure spectral noise.[62] For an ideal fit, the FQN should be close to 1.0, and the FQN/SNR ratio should be much less than 1. Some examples of linear combination model fitting are shown in Figure 5.

Linear combination model fitting is the most popular method of analysis and is recommended for most in vivo MRS applications. Several software packages provide implementations of this approach, including LCModel,[46] Tarquin,[47] Vespa,[57] FiTAID,[48] INSPECTOR[63] and jMRUI.[64] This approach is well suited to analysis of crowded MRS data, such as short-echo-time ^{1}H-MRS of the human brain, but can also be used to fit more sparse spectra, including long T_E spectra and *J*-difference edited data. Linear combination model fitting allows for the inclusion of broad macromolecular components, as well as baseline components (often a "model-free" spline function) to account for any remaining broad, unmodeled background signal contributions as described below. Since the unmodeled baseline components are poorly characterized by definition, these baseline estimates often represent the greatest source of uncertainty in fitting models. For example, the

TABLE 5 Recommendations for spectral analysis

Name of method	Recommendation
Linear combination model fitting	- generally recommended due to its proven effectiveness, versatility and relative ease of use. - ensure accuracy of the basis set: (a) for experimental basis sets derived from phantoms, the phantom temperature and pH, and the phantom acquisition parameters (pulse sequence, field strength, T_E etc.) should match the in vivo acquisition; (b) for simulated basis sets, the simulation parameters should match the in vivo acquisition (pulse sequence, field strength, echo time and optionally the RF pulse shapes and durations). (c) Simulations should use reliable estimates of chemical shifts and coupling constants of each metabolite spin system.[72-74] - always visually inspect the quality of the fit. A good fit should have small fit residuals, which mostly appear like noise. - compute the CRMVBs, which are estimators of the minimum uncertainties in the estimated parameters (assuming that the model is complete and accurate. In particular, the estimated errors will not apply if baseline estimation or phasing is done separately from actual modeling). - metabolite measures of individual subjects should not be excluded based on high relative uncertainties (% CRMVB). Instead, individual subjects may be excluded on the basis of high absolute CRMVB values. - if the average %CRMVB for a metabolite is consistently high (>30%) across all subjects, consider excluding that metabolite from the reported results across the entire subject cohort. - estimated baseline should be smooth, without fine structure or sharp peaks. - the number of protons per metabolite spin system is automatically encoded within the simulated or acquired basis set. Therefore, when using linear combination model fitting, the number of protons does NOT need to be considered in quantification (see quantification section).
Handling MM and baseline contributions	- MM fitting and baseline correction are generally required, but MM components can be omitted for long echo-time data ($T_E \geq 150$ ms at 3 T; $T_E \geq 100$ ms at 7 T; $T_E \geq 100$ ms at 9.4 T in rodent brain). - MM resonances should be removed or accounted for by including them as components in the analysis model. - ideally, MM models should be based on an acquired MM spectrum. - even with nuisance peak removal and MM modelling, an additional baseline correction should be performed. Use either time domain methods that assume rapid decay of baseline components, or frequency domain methods that assume a spline baseline.
Peak fitting and peak integration	- recommended only in cases where (a) the spectrum is sparse (contains relatively few peaks), and (b) MM and baseline contributions are minimal, or have been removed in preprocessing. - spectrum must be properly phased prior to peak integration. - peak fitting requires that spectral peaks can be approximated by simple line shape functions. Peak integration does not have this requirement. - when using peak fitting or peak integration the number of protons per metabolite peak does need to be considered in quantification (see quantification section). - in the case of peak fitting, always visually inspect the quality of the fit. A good fit should have small fit residuals and low uncertainties on peak area estimates.

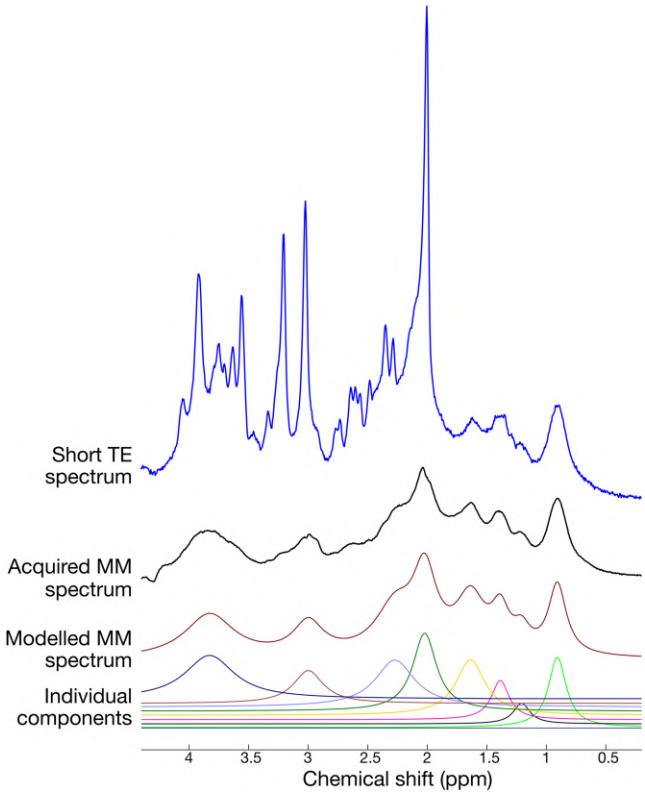

FIGURE 6 Macromolecule estimation in short-T_E MRS. The top trace (blue) shows a 3 T MR spectrum from a human subject using the SPECIAL sequence with T_E = 8.5 ms. The second trace from the top (black) shows the metabolite-nulled MM spectrum from the same individual and voxel position, obtained using the same pulse sequence, but with an inversion recovery preparation. The third trace from top (dark red) illustrates a simple model fit of the above MM spectrum using eight individual Lorentzian components. The eight individual components of the modelled MM spectrum fit are shown in the bottom traces

knot spacing of the spline function can be chosen by the user, but the choice is fairly arbitrary and can have a significant impact on metabolite concentration estimates.[65]

3.2 | Peak fitting

Rather than using basis spectra to model each metabolite's full spectral contribution, it is possible to select individual peaks of interest within a spectrum, and to fit each using a simple line shape model function. This involves choosing a line shape model that best describes the peaks of interest and fitting each spectral peak of interest to the model function. Common line shape functions include Gaussian, Lorentzian and Voigt. Fitting is achieved through adjustment of multiple model parameters including the amplitude, phase, frequency offset, linewidth and baseline offset of each model function (or of all model functions, globally); however, the main parameter of interest is the amplitude, which scales in direct proportion to concentration. For metabolites with multiple resonances, prior knowledge of the fixed relative amplitudes, phases and frequencies of the various peaks can (and should) be used to constrain the fits and improve the results. This is the method employed by the AMARES[66] technique, which is built into the popular MRS software package jMRUI.[64,67] However, in crowded spectra such as ^{1}H-MRS of the brain, the amount of prior knowledge quickly becomes overwhelming due to the large number of metabolites and the large number of peaks per metabolite. Therefore, similarly to peak integration (see below), this method is most commonly used in applications involving relatively sparse MRS data such as long T_E, or *J*-difference edited brain MRS,[68,69] phosphorus (^{31}P) MRS[70] or carbon-13 (^{13}C) MRS.[71] Compared with peak integration, peak fitting is less sensitive to baseline contamination, especially if a baseline offset parameter is included in the fit.

3.3 | Modelling of macromolecule and baseline signal

Underlying the signals of the handful of detectable small molecules (metabolites) in tissue are signals from many larger MR visible molecules (proteins, mobile lipids, etc.). These larger molecules are often called macromolecules (MM), and are characterized by short T_2 relaxation, resulting in broad spectral components that underlie the signals of interest. Because the specific molecular origins of these signals are poorly characterized, modelling of MM signals is difficult, and necessarily empirical in nature. However, if not accounted for, MM contamination will cause metabolite concentrations to be overestimated, particularly in short-echo-time ^{1}H-MRS data. Because of their relatively rapid T_2 relaxation, MM components can be omitted from the model when fitting data acquired at very long echo times (see Table 5 for recommended T_E thresholds for omitting MM).

There are various ways to account for MM contributions. One common approach is to include parametrized models of the most prominent macromolecular signals as components in the spectral fitting model.[75,76] Another common approach is to directly acquire the macromolecular signals using a metabolite-nulled (single or double) inversion recovery sequence.[77,78] Once measured directly, this MM component can either be subtracted from the metabolite spectrum prior to analysis[79,80] or included as a component in the spectral fit.[81] Figure 6 shows an example of the typical signal contribution from MM in short-echo-time MRS, and its modeling via individual parametrized components.

Even after nuisance signals and MM components have been removed from the spectrum as described above, the spectral baseline still may not appear perfectly flat. The remaining baseline arises from any unmodeled signal sources, including the long tail of an unsuppressed water peak, additional unmodeled macromolecular components, or outer volume contamination. These baseline signals should be removed prior to spectral analysis or included in the fitting model to avoid biasing metabolite concentration estimates. This baseline signal can be estimated directly from the acquired MRS data either using time domain approaches that assume very early decay,[82] or frequency domain methods that attempt to model the baseline as a spline function.[46] In any case, it is difficult to separate the baseline from the metabolite signals; and as a result this is one of the largest sources of uncertainty in in vivo MRS quantification. For further details on state-of-the-art MM modeling and baseline signal correction, the reader is referred to the experts' recommendations article on MM in this special issue.[83]

3.4 | Peak integration

Peak integration estimates a metabolite's signal intensity by calculating the area under its peak in the frequency domain.[84] This is done by choosing a frequency range around the center of the (well phased) peak of interest, and summing the discrete spectral points within this range. When quantifying multiple peaks in the same spectrum, it is important to ensure that the width of the integration range is the same for all peaks.[84] Although strictly speaking, spectral peaks have infinite extent in the frequency domain, it is generally sufficient to ensure that the integration range is at least twice the full width at half maximum (FWHM) of the broadest peak. If a spectrum is sparse with few overlapping peaks, peak integration can be robust. However, if the spectrum contains multiple overlapping peaks, peak integration cannot effectively estimate their individual contributions. Similarly, peak integrals will be biased by the presence of baseline contributions, and are unreliable for multiplet groups whose net area is close to zero (e.g., anti-phase coherences). Therefore, peak integration is only recommended for MRS data with very sparse (non-overlapping), well phased peaks and no baseline or MM contribution (e.g., ^{1}H-MRS with T_E > 150 ms, or ^{13}C spectra).

Recommendations for spectral analysis are listed in Table 5.

4 | QUANTIFICATION: FROM SIGNALS TO CONCENTRATIONS

Converting ^{1}H-MRS signals from the brain into metabolite concentrations entails comparing the metabolite signals with either an internal or external chemical concentration reference or with an externally synthesized signal. The internal references used are either the tissue water signal or an individual signal (or combination of signals) within the metabolite spectrum. The most common external standard consists of water or a chemical of known concentration in a solution either positioned close to the subject's head during the scan or scanned before or after the subject ("phantom replacement"). Less commonly, an RF signal is artificially injected during the MRS sequence detection period, using either an external antenna or a scanner RF coil (ERETIC—Electric Reference to Access in vivo Concentrations[85]—although this method is not yet available from any of the major scanner vendors).

When referenced to other metabolite signals, metabolite levels are usually reported simply as a ratio to the reference metabolite (either an intensity ratio or a concentration ratio, the distinction being that the latter is corrected for the number of protons per peak, while the former is not) and not corrected for relaxation or partial volume effects. When referenced to a known concentration standard corrected for partial volume and relaxation effects, concentrations are reported in terms of "absolute" concentrations, using either molar (moles per L of tissue) or molal units (moles per kg of tissue water). Units of moles per kg of tissue are also sometimes used and are closely related to molar units, but are not further discussed here. Alternatively, "institutional units" are often used to report relative concentration levels, making limited corrections for relaxation or claims to be the actual concentrations. As described in more detail below, our main recommendation is to use molar or molal units over institutional units; and importantly, whatever concentration units are used, it should be explicitly stated in any publication of the findings.

Though a survey of the MRS literature may reveal that molarity is reported more often than molality, both are equally valid ways of reporting concentration. Regardless of which unit is used, the difference between them is important to understand when comparing results across studies.

In chemistry, molarity is the number of moles of solute (metabolite) per volume of solution (tissue). When comparing a metabolite signal from tissue to a water or chemical signal from an external solution of known molar concentration, the appropriate units are molarity. However, when using tissue water as a reference, either molarity or molality can be used. In the case of molarity, the tissue volume sampled (excluding cerebrospinal fluid (CSF)) is considered to be the volume of the "solution." That is, the solution is the tissue water (the solvent) along with all the other components of the tissue, excluding CSF. To account for the fact that the water signal arises from only a fraction

of the solution volume, the concentration of water in the tissue is estimated by scaling the concentration of pure water by the assumed tissue water density, which differs in grey matter (GM) and white matter (WM). Molality, on the other hand, is simply based on how much solute (metabolite) is present in a mass of solvent (the tissue water), and thus may relate more closely to the chemical concentration (i.e., intracellular concentration). As will be shown in the following section, if the MRS signals are not acquired under fully relaxed conditions, the tissue densities also need to be taken into account to properly scale for relaxation attenuation in different compartments when estimating either molarity or molality.

4.1 | Internal references

4.1.1 | Tissue water

The most commonly used reference for estimating metabolite concentrations is the tissue water signal.[86-89] An advantage of using the water signal is that it arises from essentially the same volume of tissue as the metabolite when the same pulse sequence is used to acquire the metabolite signals. This ensures that the RF calibration and homogeneity, excitation profile and receiver sensitivity at the location of the metabolite and water acquisitions are identical. This is approximately the case for single-voxel ^{1}H-MRS if the chemical shift displacement is minimized.

The cellular environments of the metabolites are complex and varied, with different water, MM and lipid densities, and other factors affecting signal relaxation and detection. To make the problem tractable, the first assumption generally made is that the various metabolite compartments can be approximated as GM, WM, CSF and possibly pathological tissue (e.g., MRI-visible lesions), with uniform physical properties within each of these pools, including across cellular and extracellular sub-compartments. The different tissue and CSF fractions are determined by segmentation of an MR image to which the MRS voxel has been registered. It is worth noting that different MRI segmentation methods generally give slightly different results, and there is no "gold standard" to establish their relative accuracy.[90]

In a simple solution, the ^{1}H-MRS signal from a solute (or from the solvent) is directly proportional to the number of moles of the solute (or of solvent) in the sampled voxel, scaled by any relaxation attenuation and instrumental factors (see the work of Alger[91] for a comprehensive review). In the complex milieu of brain tissue, it is usually assumed that all of the molecules of a metabolite of interest contribute to the measured signal. This implies that the molecules are mobile enough to have a relatively long T_2, and hence relatively narrow spectral peak(s). When correcting a multi-peak metabolite signal for relaxation, it is often (but not always) assumed that the signals from distinct protons on the molecule, aside from any exchangeable ones, have the same T_2 and T_1.

For the case of fully relaxed water and metabolite proton signals acquired identically from the same volume of pure tissue (i.e., no CSF), we can write

$$\frac{S_M}{S_{H2O}} = \frac{\text{moles of metabolite} \times N_M}{\text{moles of water} \times 2} \tag{1}$$

where S_M and S_{H2O} are the metabolite and water proton signal intensities, respectively, N_M is the number of metabolite protons contributing to S_M and 2 is the number of water protons contributing to S_{H2O}. In the case of linear combination model fitting, the number of protons (N_M and the factor of 2 in the denominator) can safely be ignored here and in the equations that follow, since these values are encoded in the relative amplitudes of the peaks in the basis spectra.

To convert the signal ratio in Equation (1) to units of concentration, we divide both mole factors by either the mass of the solvent (tissue water) for molal concentrations or liters of solution (total tissue) for molar concentrations and rearrange the equation. For molality, $[M]_{molal}$, this becomes

$$[M]_{molal} = \frac{S_M}{S_{H2O}} \frac{2}{N_M} [H_2O]_{molal} \tag{2}$$

where $[H_2O]_{molal}$ is the molal concentration of pure water or 55.51 moles/kg, the inverse of its molecular weight (18.015×10^3 kg/mole, https://pubchem.ncbi.nlm.nih.gov/compound/Water).

If molar concentration is to be estimated, the total volume of sampled tissue needs to be considered rather than just the volume of tissue water. In order to account for the fact that the water signal arises from only a fraction of the tissue volume, the molar concentration of tissue water is estimated by scaling the molar concentration of pure water by the tissue water density, which differs in GM and WM. Again assuming a voxel with pure tissue (no CSF), the molar concentration based on fully relaxed signals is calculated as

$$[M]_{molar} = \frac{S_M}{S_{H2O}} (f_{GM} d_{GM} + f_{WM} d_{WM}) \frac{2}{N_M} [H_2O]_{molar} \tag{3}$$

where d_{GM} and d_{WM} refer to the tissue-specific water content, defined as the MR visible water volume fraction in either GM or WM (see Appendix I in Supporting Information), f_{GM} and f_{WM} are the volume fractions of GM and WM in the voxel and $[H_2O]_{molar}$ is approximately 55.01 moles/L at 37°C and 1 bar of pressure. Values for water content in healthy human brain tissue have been drawn from various reports,[87] but it is well to

keep in mind that, regardless of the source, one set of water density values may not be appropriate for the entire brain or for pathological tissue.[92] In particular, in WM it should be considered whether and to what degree the short-T_2 pool of myelin water[93] of up to 15% is contributing to the water reference signal.[87]

If the voxel contains CSF, the water concentration in Equation (2) is divided by the tissue water mole fraction in the voxel ($f_{GM_{H2O}} + f_{WM_{H2O}}$ or equivalently $1-f_{CSF_{H2O}}$, where $f_{CSF_{H2O}}$ is the CSF water mole fraction). Similarly, $[M]_{molar}$ in Equation (3) needs to be scaled by the volume fraction of tissue ($f_{GM} + f_{WM}$, or equivalently $1 - f_{CSF}$, where f_{CSF} is the CSF volume fraction), and the term multiplying the signal ratio becomes ($f_{GM}d_{GM}+f_{WM}d_{WM}+f_{CSF}d_{CSF}$). CSF is generally devoid of detectable metabolites in healthy brain other than glucose (3–5mM), lactate (~2mM)[94,95] and glutamine (0.4–0.8mM),[96,97] and the contributions of even these metabolites are usually assumed to be insignificant if care is taken to minimize the fraction of CSF in the voxel (e.g., $f_{CSF} < 0.2$).

Taking into consideration the effect of signal relaxation leads to the final modifications of the fundamental equations (2) and (3). If the data were not acquired under fully relaxed conditions, the observed signals, $S_{M_{obs}}$ and $S_{H2O_{obs}}$, need to be divided by appropriate relaxation factors. In the case of a typical double spin echo (e.g., PRESS) or stimulated echo experiment (e.g., STEAM) with $T_R \gg T_E$, the form of the relaxation scaling factors is $R = \exp(-T_E/T_2)[1 - \exp(-T_R/T_1)]$, where the relaxation times are those of either the metabolite or the water protons. If T_R is not much greater than T_E, the factor is $R = \exp(-T_E/T_2)\{1-2\exp[-(T_R - T_{E1}/2)/T_1] + 2\exp[-(T_R - T_{E1} - T_{E2}/2)/T_1] - \exp(-T_R/T_1)\}$,[98,99] where T_{E1} and T_{E2} are the first and second echo times within the double-echo pulse sequence.

Water proton signals relax at different rates in GM, WM and CSF, as do metabolite proton signals in GM and WM. The differences are large for water, spanning a factor of nearly 10 from WM to CSF. However, they are comparatively small for metabolites in GM and WM, such that the metabolite relaxation times can be approximated as the average of their GM and WM times without adding a large error to the concentration estimate.[100] Accounting for tissue-specific water relaxation as well as a partial volume correction for CSF leads to the following expression for molal concentration[90]:

$$[M]_{molal} = \frac{S_{M_{obs}}\left(f_{GM_{H2O}}R_{H2O_{GM}} + f_{WM_{H2O}}R_{H2O_{WM}} + f_{CSF_{H2O}}R_{H2O_{CSF}}\right)}{S_{H2O_{obs}}\left(1-f_{CSF_{H2O}}\right)R_M}\frac{2}{N_M}[H_2O]_{molal} \quad (4)$$

where the relaxation scaling factors R_{H2O_x} refer to the factors for water protons in GM, WM or CSF, and the term R_M refers to the relaxation scaling factor for metabolite protons assuming average GM-WM relaxation times or, in the case of voxels with CSF and only GM or only WM, the metabolite relaxation times appropriate to either tissue.

As noted above, the fractions appearing in this equation are the tissue and CSF water mole fractions. They are related to the tissue volume fractions (obtained by image segmentation) according to the following equation:

$$f_{x_{H2O}} = \frac{f_x d_x}{f_{GM}d_{GM} + f_{WM}d_{WM} + f_{CSF}d_{CSF}} \quad (5)$$

where x in the subscript refers to GM, WM or CSF. Converting from tissue volume to tissue water mole fractions using Equation (5) relies on assumptions of water density, often taken to be $d_{GM} = 0.78$, $d_{WM} = 0.65$ and $d_{CSF} = 0.97$.[87]

An equation similar to Equation (4) can be derived for molar concentrations[100,101]:

$$[M]_{molar} = \frac{S_{M_{obs}}\left(f_{GM}d_{GM}R_{H2O_{GM}} + f_{WM}d_{WM}R_{H2O_{WM}} + f_{CSF}d_{CSF}R_{H2O_{CSF}}\right)}{S_{H2O_{obs}}\left(1-f_{CSF}\right)R_M}\frac{2}{N_M}[H_2O]_{molal}. \quad (6)$$

Equations (4) and (6) can be further modified using Equation (7) below to include tissue-specific (GM and WM) relaxation scaling factors for metabolites[100]:

$$R_{M_{GM_{WM}}} = \frac{f_{GM}d_{GM}\left([M]_{GM}/[M]_{WM}\right)R_{M_{GM}} + f_{WM}d_{WM}R_{M_{WM}}}{f_{GM}d_{GM}\left([M]_{GM}/[M]_{WM}\right) + f_{WM}d_{WM}}. \quad (7)$$

This term introduces an extra unknown factor, $[M]_{GM}/[M]_{WM}$, i.e., the ratio of the GM to the WM metabolite concentrations, which is not known a priori. The ratio arises from the need to know what fraction of the total metabolite signal is to be weighted by $R_{M_{GM}}$ and what fraction by $R_{M_{WM}}$. For a detailed derivation of the above quantification formulae, the reader is referred to Appendix I (Supporting Information).

Using Equations (4) and (7) with simulated 3 T data and assuming metabolite ratios from previous studies, it was shown that the errors that arise from not correcting for tissue-specific metabolite relaxation in mixed-tissue voxels will be less than 8% for *N*-acetylaspartate (NAA) when assuming typical T_R and T_E values, reported GM and WM metabolite relaxation times and a hypothetical GM/WM NAA ratio of 1.2.[100] For example, maximum errors of 7.8% in concentrations resulted when $T_R = 1.5$ s and $T_E = 144$ ms, but were reduced to 1.6% when $T_R = 3$ s and $T_E = 6$ ms and to less than 0.5% when $T_R = 6$ s and $T_E = 6$ ms. The maximum errors occur when the tissue-averaged relaxation times are used instead of the

tissue-specific relaxation times to "correct" the relaxation attenuation when the voxel actually contains only pure GM or pure WM. Equation (7) can be used to examine the possible errors arising in any other scenario.

To minimize such errors, accurate estimates of tissue-specific metabolite relaxation times, when available, should be used to correct for relaxation attenuation in voxels with mixtures of GM and WM. It is worth noting, however, that metabolite relaxation times are very challenging to measure, even for metabolites with relatively high SNR, and are simply not practical to perform for all metabolites of interest, or in every region of the brain or on a study-to-study basis. Furthermore, both water and tissue relaxation times are field dependent and brain metabolite relaxation times have been reported to vary with age.[102-104]

In lieu of accurate relaxation time estimates, long T_R ($T_R \gg T_1$) and short T_E ($T_E \ll T_2$) should be considered to reduce relaxation attenuation when possible, as illustrated in the case of NAA shown above. However, the T_E used in a study is often determined by the specific pulse sequence applied, which depends on the goals of the study (e.g., spectral editing or otherwise optimizing detection of particular signals, reduction of high-field artefacts with adiabatic pulses etc). Moreover, the T_R needs to be short enough (usually ≤3 s) to be practical for human studies. If a long T_R and short T_E are not possible, ensuring that the MRS voxel contains mostly GM or mostly WM and using the metabolite relaxation times appropriate to that tissue will be the best option for reducing errors due to inaccurate relaxation times.

The recommendations for reducing errors related to inaccurate metabolite relaxation time estimates also apply to inaccuracies in the estimates of the water signal relaxation times. Long T_R and short T_E values reduce the effect of these inaccuracies. A field-independent T_1 of approximately 4 s has been reported for CSF water protons,[105] so the CSF water signal will still be appreciably attenuated even at a T_R of 3 s. Therefore, care should be taken to minimize the fraction of CSF in the voxel to reduce the CSF water signal contribution. Additionally, it is worth noting that if molal concentrations are estimated the impact of inaccurate assumptions about the tissue water densities are reduced at long T_R and short T_E, vanishing as the relaxation factors in Equation (4) approach a value of 1.

Given the challenges for accurate ^{1}H-MRS concentration estimates in the brain, it is not surprising that some researchers opt for reporting "institutional units," making no claim to be the actual concentration. Such units are fine when comparing different groups within a study, given the caveats on the interpretation of the results noted above. However, attempting to estimate the actual concentrations facilitates the comparison of results across studies and field strengths, essential for meta-analyses. Due to the challenges discussed above, particularly the unknown variation of water density and signal relaxation with pathology, this will be difficult to realize in practice. However, if MRS is ever to be used as a routine clinical examination, similar to a blood test, concentration estimates based on some standard protocol would be desirable.

4.1.2 | Metabolite ratios

In principle, using either the water signal or another metabolite signal within the spectrum as a concentration reference are both "ratio" methods. The water signal is about 10^4 times larger than the metabolite signals and is uncomplicated by overlap with other signals, whereas any metabolite reference is, by comparison, very weak and has to be resolved from its spectral neighbors. Furthermore, it is not possible to minimize the chemical shift displacement error inherent across the spectrum by changing the excitation frequency of the reference signal, as in tissue water referencing. However, a reference signal from within the metabolite spectrum (from either a single or a sum of metabolites) shares the other benefits of tissue water as a reference: it is inherently corrected for transmit RF field (B_1) and receiver inhomogeneity, magnetic field drift and other instrumental factors. Additionally, a metabolite reference has two advantages over tissue water: (1) no extra scan is needed to obtain it and (2) it obviates the need to correct the results for CSF inclusion in the voxel, since, as noted previously, other than lactate and glucose, the metabolites in CSF are generally below the levels of detection by in vivo ^{1}H-MRS if care is taken to minimize its inclusion in the voxel.

TABLE 6 Recommendations for quantification referenced to water

Method	Recommendations
Reference signal and quantification units	- comparing metabolite signals to tissue water within the same region of interest, and calculating concentrations in either molarity or molality, is the most robust and technically straightforward approach to "absolute" quantification. - whatever concentrations are used, this must be explicitly stated in any publication of the findings; preferably along with the specific quantification formulae that were used as well all assumed parameter values, so that the reader can fully reproduce the quantification method.
T_E and T_R	- while short T_E and long T_R values are not an option for many pulse sequences, if absolute concentration estimates are a goal of the study pulse sequences capable of very short T_E values, such as STEAM[119] or SPECIAL,[29] could be considered. - if short T_E (<10 ms) and/or long T_R (> 4 s) is not possible, measured or literature values of the metabolite and water relaxation constants (T_1, T_2) should be used in quantification. - all assumed values for relaxation constants, tissue water densities etc. must be reported, so that others may compare results.
ERETIC	- the ERETIC method, while promising, is not yet widely available. We encourage scanner manufacturers to develop ERETIC referencing capabilities in their products, which we believe would be an important step towards reliable absolute quantification on clinical systems.

An important factor to consider when using metabolite ratios is confidence in the stability of the reference across age, gender, pathology or other factors. As noted earlier, while the concentration of pure water does not change (molarity does change with temperature and pressure, molality does not), the tissue water density may in fact change with pathology or other factors.[106] Similarly, the metabolite signals typically used as references, such as those from the total creatine (tCr = Cr (creatine) + PCr (phosphocreatine)), total choline (tCho = GPC (glycerophosphocholine) + PCh (phosphocholine)) or total *N*-acetylaspartate (tNAA = NAA + NAAG (*N*-acetylaspartylglutamate)), are also subject to change with age[81,107-109] and pathology.[110-113]

The majority of studies reporting metabolite ratios use the tCr signal as the reference, with the results given as the values of the ratio and not as concentrations. The latter option would require an assumption about the concentration of tCr which, in fact, would need to take into consideration its very different concentrations in GM and WM (GM [tCr] is nearly double WM [tCr]). Along these lines, generally no correction is made for GM and WM partial volume effects or tissue-specific relaxation effects. Hence, metabolite ratios, while circumventing the needs for CSF partial volume correction and a separate acquisition to measure the reference (as is done for water referencing), are not concentration estimates per se. They are conveniently acquired markers of metabolic differences, their interpretation subject to assumptions regarding which part of the ratio is changing, if not both, and in which direction.

4.2 | External references

4.2.1 | External solution

The most common approach to referencing the metabolites of the brain to an external reference involves scanning a spherical "phantom" solution containing a particular concentration of the reference chemical after scanning the brain (phantom replacement or reciprocity principle).[114,115] Less commonly, a phantom solution is located next to the subject's head during the scan. Either method requires correcting the signals for differences in RF power (coil loading and B_1 inhomogeneity) and/or receiver sensitivity between the phantom and brain voxel locations, introducing possible instrumental sources of error. Notably, variations in B_1 homogeneity are more likely at high B_0 field strength, largely limiting its use to 3 T and below. In addition to these, of course, one must still be concerned about partial volume and signal relaxation corrections, as discussed for internal standards, if accurate concentration estimates are desired.

4.2.2 | ERETIC

ERETIC entails the synthesis of a calibrated RF signal close in frequency to the metabolite signals and detected either along with metabolite signals[85,116,117] or in a separate experiment.[118] The synthesized signal is either broadcast by a scanner coil or an external antenna[85,118] or it is directly inductively coupled to the receiver coil.[116,117] The signal is calibrated with a water phantom with similar size and dielectric properties to the head. However, unlike using the phantom directly as a reference for the metabolite signal, the synthesized signal does not dielectrically load the ^{1}H receiver coil and, hence, does not need to be corrected for different loading. Transmit RF (B_1) inhomogeneity and receiver sensitivity differences between the brain and phantom acquisitions, however, still need to be measured and accounted for in the calculation of concentrations, as does the phase of the synthesized signal and the temperature difference between the phantom and brain.[117] Currently, the development of ERETIC has been limited to single-voxel studies. The need for accurate partial volume and relaxation corrections, as when using tissue water as an internal reference, remain. Three different studies have shown that ERETIC measurements of brain metabolites compare well with those based on tissue water as a concentration reference.[116-118]

Recommendations for absolute quantification are listed in Table 6.

5 | CONCLUSIONS

In conclusion, preprocessing, analysis and quantification are the three main steps in the post-acquisition MRS workflow. Each of these steps is challenging, and requires careful thought and planning in order to achieve the end goal of obtaining reliable quantitative measures of tissue chemistry. It is hoped that the guidelines and recommendations provided here will serve as a useful resource to inform on best practices and to warn of the pitfalls that are commonly encountered.

ACKNOWLEDGEMENTS

The authors wish to acknowledge the following sources of support. JN is supported by the Natural Sciences and Engineering Research Council of Canada (RGPIN-2014-06072), the Canadian Institutes of Health Research (PJT-148751, PJT-165869) and the Fonds de Recherche du Québec—

Santé (FRQ: 0000035275). ADH is supported by the Natural Sciences and Engineering Research Council of Canada (RGPIN-2017-03875). RK is supported by the Swiss National Science Foundation (Schweizerischer Nationalfonds 320030-175984). GÖ is supported by the National Institute of Neurological Disorders and Stroke (R01 NS080816). MM and the Centre for Magnetic Resonance Research are supported by the National Institute of Biomedical Imaging and Bioengineering (P41 EB015894) and the Institutional Centre Cores for Advanced Neuroimaging award (P30 NS076408).

ORCID

Jamie Near https://orcid.org/0000-0003-3516-936X
Ashley D. Harris https://orcid.org/0000-0003-4731-7075
Christoph Juchem https://orcid.org/0000-0002-1505-201X
Roland Kreis https://orcid.org/0000-0002-8618-6875
Małgorzata Marjańska https://orcid.org/0000-0002-4727-2447
Gülin Öz https://orcid.org/0000-0002-5769-183X
Johannes Slotboom https://orcid.org/0000-0001-5121-9852
Martin Wilson https://orcid.org/0000-0002-2089-3956
Charles Gasparovic https://orcid.org/0000-0002-4433-7815

REFERENCES

1. Maudsley AA. Advanced magnetic resonance spectroscopic neuroimaging techniques: experts' consensus recommendations. *NMR Biomed*. In press
2. Inati SJ, Naegele JD, Zwart NR, et al. ISMRM raw data format: a proposed standard for MRI raw datasets. *Magn Reson Med*. 2017;77:411-421.
3. Klose U. In vivo proton spectroscopy in presence of eddy currents. *Magn Reson Med*. 1990;14:26-30.
4. de Graaf AA, van Dijk JE, Bovee WM. QUALITY: quantification improvement by converting lineshapes to the Lorentzian type. *Magn Reson Med*. 1990;13:343-357.
5. Bartha R, Drost DJ, Menon RS, Williamson PC. Spectroscopic lineshape correction by QUECC: combined QUALITY deconvolution and eddy current correction. *Magn Reson Med*. 2000;44:641-645.
6. Hess AT, Tisdall MD, Andronesi OC, Meintjes EM, van der Kouwe AJ. Real-time motion and B_0 corrected single voxel spectroscopy using volumetric navigators. *Magn Reson Med*. 2011;66:314-323.
7. Hess AT, Jacobson SW, Jacobson JL, Molteno CD, van der Kouwe AJ, Meintjes EM. A comparison of spectral quality in magnetic resonance spectroscopy data acquired with and without a novel EPI-navigated PRESS sequence in school-aged children with fetal alcohol spectrum disorders. *Metab Brain Dis*. 2014;29:323-332.
8. Hess AT, van der Kouwe AJ, Mbugua KK, Laughton B, Meintjes EM. Quality of 186 child brain spectra using motion and B0 shim navigated single voxel spectroscopy. *J Magn Reson Imaging*. 2014;40:958-965.
9. Hess AT, Andronesi OC, Tisdall MD, Sorensen AG, van der Kouwe AJ, Meintjes EM. Real-time motion and B_0 correction for localized adiabatic selective refocusing (LASER) MRSI using echo planar imaging volumetric navigators. *NMR Biomed*. 2012;25:347-358.
10. Saleh MG, Alhamud A, Near J, van der Kouwe AJ, Meintjes EM. Volumetric navigated MEGA-SPECIAL for real-time motion and shim corrected GABA editing. *NMR Biomed*. 2016;29:248-255.
11. Zaitsev M, Speck O, Hennig J, Buchert M. Single-voxel MRS with prospective motion correction and retrospective frequency correction. *NMR Biomed*. 2010;23:325-332.
12. Andrews-Shigaki BC, Armstrong BS, Zaitsev M, Ernst T. Prospective motion correction for magnetic resonance spectroscopy using single camera retro-grate reflector optical tracking. *J Magn Reson Imaging*. 2011;33:498-504.
13. Lange T, Maclaren J, Buechert M, Zaitsev M. Spectroscopic imaging with prospective motion correction and retrospective phase correction. *Magn Reson Med*. 2012;67:1506-1514.
14. Kreis R. Issues of spectral quality in clinical ^{1}H-magnetic resonance spectroscopy and a gallery of artifacts. *NMR Biomed*. 2004;17:361-381.
15. Simpson R, Devenyi GA, Jezzard P, Hennessy TJ, Near J. Advanced processing and simulation of MRS data using the FID appliance (FID-A)—an open source, MATLAB-Based Toolkit. *Magn Reson Med*. 2017;77:23-33.
16. Slotboom J, Nirkko A, Brekenfeld C, van Ormondt D. Reliability testing of *in vivo* magnetic resonance spectroscopy (MRS) signals and signal artifact reduction by order statistic filtering. *Meas Sci Technol*. 2009;20:104030.
17. El-Sharkawy AM, Schar M, Bottomley PA, Atalar E. Monitoring and correcting spatio-temporal variations of the MR scanner's static magnetic field. *Magn Reson Mater Phys Biol Med*. 2006;19:223-236.
18. Star-Lack JM, Adalsteinsson E, Gold GE, Ikeda DM, Spielman DM. Motion correction and lipid suppression for ^{1}H magnetic resonance spectroscopy. *Magn Reson Med*. 2000;43:325-330.
19. Helms G, Piringer A. Restoration of motion-related signal loss and line-shape deterioration of proton MR spectra using the residual water as intrinsic reference. *Magn Reson Med*. 2001;46:395-400.
20. Henry PG, van de Moortele PF, Giacomini E, Nauerth A, Bloch G. Field-frequency locked in vivo proton MRS on a whole-body spectrometer. *Magn Reson Med*. 1999;42:636-642.
21. Keating B, Deng W, Roddey JC, et al. Prospective motion correction for single-voxel ^{1}H MR spectroscopy. *Magn Reson Med*. 2010;64:672-679.
22. Thiel T, Czisch M, Elbel GK, Hennig J. Phase coherent averaging in magnetic resonance spectroscopy using interleaved navigator scans: compensation of motion artifacts and magnetic field instabilities. *Magn Reson Med*. 2002;47:1077-1082.
23. Waddell KW, Avison MJ, Joers JM, Gore JC. A practical guide to robust detection of GABA in human brain by J-difference spectroscopy at 3 T using a standard volume coil. *Magn Reson Imaging*. 2007;25:1032-1038.

24. Near J, Edden R, Evans CJ, Paquin R, Harris A, Jezzard P. Frequency and phase drift correction of magnetic resonance spectroscopy data by spectral registration in the time domain. *Magn Reson Med*. 2015;73:44-50.
25. Wilson M. Robust retrospective frequency and phase correction for single-voxel MR spectroscopy. *Magn Reson Med*. 2019;81:2878-2886.
26. Wiegers EC, Philips BWJ, Heerschap A, van der Graaf M. Automatic frequency and phase alignment of in vivo J-difference-edited MR spectra by frequency domain correlation. *Magn Reson Mater Phys Biol Med*. 2017;30:537-544.
27. Tapper S, Tisell A, Helms G, Lundberg P. Retrospective artifact elimination in MEGA-PRESS using a correlation approach. *Magn Reson Med*. 2019;81:2223-2237.
28. Dreher W, Leibfritz D. New method for the simultaneous detection of metabolites and water in localized in vivo ^{1}H nuclear magnetic resonance spectroscopy. *Magn Reson Med*. 2005;54:190-195.
29. de Graaf RA, Sacolick LI, Rothman DL. Water and metabolite-modulated MR spectroscopy and spectroscopic imaging. *Proc Int Soc Magn Reson Med*. 2006;14:3063.
30. Hock A, MacMillan EL, Fuchs A, et al. Non-water-suppressed proton MR spectroscopy improves spectral quality in the human spinal cord. *Magn Reson Med*. 2013;69:1253-1260.
31. Emir UE, Burns B, Chiew M, Jezzard P, Thomas MA. Non-water-suppressed short-echo-time magnetic resonance spectroscopic imaging using a concentric ring *k*-space trajectory. *NMR Biomed*. 2017;30:e3714.
32. Mescher M, Merkle H, Kirsch J, Garwood M, Gruetter R. Simultaneous in vivo spectral editing and water suppression. *NMR Biomed*. 1998;11:266-272.
33. Chan KL, Puts NA, Schar M, Barker PB, Edden RA. HERMES: Hadamard encoding and reconstruction of MEGA-edited spectroscopy. *Magn Reson Med*. 2016;76:11-19.
34. Mekle R, Mlynarik V, Gambarota G, Hergt M, Krueger G, Gruetter R. MR spectroscopy of the human brain with enhanced signal intensity at ultrashort echo times on a clinical platform at 3T and 7T. *Magn Reson Med*. 2009;61:1279-1285.
35. Puts NA, Harris AD, Crocetti D, et al. Reduced GABAergic inhibition and abnormal sensory symptoms in children with Tourette syndrome. *J Neurophysiol*. 2015;114:808-817.
36. Porges EC, Woods AJ, Edden RA, et al. Frontal gamma-aminobutyric acid concentrations are associated with cognitive performance in older adults. *Biol Psychiatry Cogn Neurosci Neuroimaging*. 2017;2:38-44.
37. Evans CJ, Puts NA, Robson SE, et al. Subtraction artifacts and frequency (mis-)alignment in *J*-difference GABA editing. *J Magn Reson Imaging*. 2013;38:970-975.
38. Cleve M, Kramer M, Gussew A, Reichenbach JR. Difference optimization: automatic correction of relative frequency and phase for mean non-edited and edited GABA ^{1}H MEGA-PRESS spectra. *J Magn Reson*. 2017;279:16-21.
39. Mikkelsen M, Saleh MG, Near J, et al. Frequency and phase correction for multiplexed edited MRS of GABA and glutathione. *Magn Reson Med*. 2018;80:21-28.
40. van der Veen JW, Marenco S, Berman KF, Shen J. Retrospective correction of frequency drift in spectral editing: the GABA editing example. *NMR Biomed*. 2017;30:e3725.
41. Choi C. Spectral editing in 1H magnetic resonance spectroscopy: experts' consensus recommendations. *NMR Biomed*. In press
42. Cabanes E, Confort-Gouny S, Le Fur Y, Simond G, Cozzone PJ. Optimization of residual water signal removal by HLSVD on simulated short echo time proton MR spectra of the human brain. *J Magn Reson*. 2001;150:116-125.
43. Pijnappel WWF, van den Boogaart A, de Beer R, van Ormondt D. SVD-based quantification of magnetic resonance signals. *J Magn Reson*. 1992;97:122-134.
44. Landheer K, Juchem C. Dephasing optimization through coherence order pathway selection (DOTCOPS) for improved crusher schemes in MR spectroscopy. *Magn Reson Med*. 2019;81:2209-2222.
45. Kyathanahally SP, Doring A, Kreis R. Deep learning approaches for detection and removal of ghosting artifacts in MR spectroscopy. *Magn Reson Med*. 2018;80:851-863.
46. Provencher SW. Estimation of metabolite concentrations from localized in vivo proton NMR spectra. *Magn Reson Med*. 1993;30:672-679.
47. Wilson M, Reynolds G, Kauppinen RA, Arvanitis TN, Peet AC. A constrained least-squares approach to the automated quantitation of in vivo ^{1}H magnetic resonance spectroscopy data. *Magn Reson Med*. 2011;65:1-12.
48. Chong DG, Kreis R, Bolliger CS, Boesch C, Slotboom J. Two-dimensional linear-combination model fitting of magnetic resonance spectra to define the macromolecule baseline using FiTAID, a fitting tool for arrays of interrelated datasets. *Magn Reson Mater Phys Biol Med*. 2011;24:147-164.
49. Hall EL, Stephenson MC, Price D, Morris PG. Methodology for improved detection of low concentration metabolites in MRS: optimised combination of signals from multi-element coil arrays. *Neuroimage*. 2014;86:35-42.
50. Roemer PB, Edelstein WA, Hayes CE, Souza SP, Mueller OM. The NMR phased array. *Magn Reson Med*. 1990;16:192-225.
51. Binczyk F, Tarnawski R, Polanska J. Strategies for optimizing the phase correction algorithms in nuclear magnetic resonance spectroscopy. *Biomed Eng Online*. 2015;14(Suppl 2):S5.
52. de Brouwer H. Evaluation of algorithms for automated phase correction of NMR spectra. *J Magn Reson*. 2009;201:230-238.
53. Chen L, Weng Z, Goh L, Garland M. An efficient algorithm for automatic phase correction of NMR spectra based on entropy minimization. *J Magn Reson*. 2002;158:164-168.
54. Menze BH, Kelm BM, Weber MA, Bachert P, Hamprecht FA. Mimicking the human expert: pattern recognition for an automated assessment of data quality in MR spectroscopic images. *Magn Reson Med*. 2008;59:1457-1466.
55. Pedrosa de Barros N, McKinley R, Knecht U, Wiest R, Slotboom J. Automatic quality control in clinical ^{1}H MRSI of brain cancer. *NMR Biomed*. 2016;29:563-575.
56. Kyathanahally SP, Mocioiu V, Pedrosa de Barros N, et al. Quality of Clinical Brain Tumor MR Spectra Judged by Humans and Machine Learning Tools. *Magn Reson Med*. 2018;79:2500-2510.
57. Soher BJ, Semanchuk P, Todd S, Steinberg J, Young K. VeSPA: integrated applications for RF pulse design, spectral simulation and MRS data analysis. *Proc Int Soc Magn Reson Med*. 2011;19:1410.
58. Smith SA, Levante TO, Meier BH, Ernst RR. Computer simulations in magnetic resonance. An object-oriented programming approach. *J Magn Reson a*. 1994;106:75-105.

59. Ratiney H, Sdika M, Coenradie Y, Cavassila S, van Ormondt D, Graveron-Demilly D. Time-domain semi-parametric estimation based on a metabolite basis set. *NMR Biomed*. 2005;18:1-13.
60. Choi C, Ganji SK, DeBerardinis RJ, et al. 2-hydroxyglutarate detection by magnetic resonance spectroscopy in IDH-mutated patients with gliomas. *Nat Med*. 2012;18:624-629.
61. Landheer K, Swanberg KM, Juchem C. Magnetic resonance Spectrum simulator (MARSS), a novel software package for fast and computationally efficient basis set simulation [published online ahead of print July 17, 2019]. *NMR Biomed*. https://doi.org/10.1002/nbm.4129
62. Slotboom J, Boesch C, Kreis R. Versatile frequency domain fitting using time domain models and prior knowledge. *Magn Reson Med*. 1998;39:899-911.
63. Columbia Technology Ventures (CTV). *INSPECTOR*: *Magnetic Resonance Spectroscopy Software for Optimized Data Extraction*. 2016. innovation.columbia.edu/technologies/cu17130_inspector.
64. Stefan D, Di Cesare F, Andrasescu A, et al. Quantitation of magnetic resonance spectroscopy signals: the jMRUI software package. *Meas Sci Technol*. 2009;20:104035.
65. Deelchand DK, Marjanska M, Hodges JS, Terpstra M. Sensitivity and specificity of human brain glutathione concentrations measured using short-TE ^{1}H MRS at 7 T. *NMR Biomed*. 2016;29:600-606.
66. Vanhamme L, van den Boogaart A, Van Huffel S. Improved method for accurate and efficient quantification of MRS data with use of prior knowledge. *J Magn Reson*. 1997;129:35-43.
67. Naressi A, Couturier C, Devos JM, et al. Java-based graphical user interface for the MRUI quantitation package. *Magn Reson Mater Phys Biol Med*. 2001;12:141-152.
68. Edden RA, Puts NA, Harris AD, Barker PB, Evans CJ. Gannet: a batch-processing tool for the quantitative analysis of gamma-aminobutyric acid-edited MR spectroscopy spectra. *J Magn Reson Imaging*. 2014;40:1445-1452.
69. Near J, Ho YC, Sandberg K, Kumaragamage C, Blicher JU. Long-term reproducibility of GABA magnetic resonance spectroscopy. *Neuroimage*. 2014;99:191-196.
70. van der Veen JW, de Beer R, Luyten PR, van Ormondt D. Accurate quantification of *in vivo* ^{31}P NMR signals using the variable projection method and prior knowledge. *Magn Reson Med*. 1988;6:92-98.
71. Lanz B, Duarte JM, Kunz N, Mlynarik V, Gruetter R, Cudalbu C. Which prior knowledge? Quantification of in vivo brain ^{13}C MR spectra following ^{13}C glucose infusion using AMARES. *Magn Reson Med*. 2013;69:1512-1522.
72. Govindaraju V, Young K, Maudsley AA. Proton NMR chemical shifts and coupling constants for brain metabolites. *NMR Biomed*. 2000;13:129-153.
73. Govind V, Young K, Maudsley AA. Corrigendum: proton NMR chemical shifts and coupling constants for brain metabolites. Govindaraju V, Young K, Maudsley AA, *NMR Biomed.* 2000; 13: 129-153. *NMR Biomed*. 2015;28:923-924.
74. Near J, Evans CJ, Puts NA, Barker PB, Edden RA. J-difference editing of gamma-aminobutyric acid (GABA): simulated and experimental multiplet patterns. *Magn Reson Med*. 2013;70:1183-1191.
75. Seeger U, Klose U, Mader I, Grodd W, Nagele T. Parameterized evaluation of macromolecules and lipids in proton MR spectroscopy of brain diseases. *Magn Reson Med*. 2003;49:19-28.
76. Povazan M, Strasser B, Hangel G, et al. Simultaneous mapping of metabolites and individual macromolecular components via ultra-short acquisition delay ^{1}H MRSI in the brain at 7T. *Magn Reson Med*. 2018;79:1231-1240.
77. Behar KL, Rothman DL, Spencer DD, Petroff OA. Analysis of macromolecule resonances in ^{1}H NMR spectra of human brain. *Magn Reson Med*. 1994;32:294-302.
78. Cudalbu C, Mlynarik V, Gruetter R. Handling macromolecule signals in the quantification of the neurochemical profile. *J Alzheimers Dis*. 2012;31 (Suppl 3):S101-S115.
79. Penner J, Bartha R. Semi-LASER ^{1}H MR spectroscopy at 7 tesla in human brain: metabolite quantification incorporating subject-specific macromolecule removal. *Magn Reson Med*. 2015;74:4-12.
80. Kassem MN, Bartha R. Quantitative proton short-echo-time LASER spectroscopy of normal human white matter and hippocampus at 4 tesla incorporating macromolecule subtraction. *Magn Reson Med*. 2003;49:918-927.
81. Marjanska M, McCarten JR, Hodges J, et al. Region-specific aging of the human brain as evidenced by neurochemical profiles measured noninvasively in the posterior cingulate cortex and the occipital lobe using ^{1}H magnetic resonance spectroscopy at 7 T. *Neuroscience*. 2017;354:168-177.
82. Ratiney H, Coenradie Y, Cavassila S, van Ormondt D, Graveron-Demilly D. Time-domain quantitation of ^{1}H short echo-time signals: background accommodation. *Magn Reson Mater Phys Biol Med*. 2004;16:284-296.
83. Cudalbu C. Contribution of macromolecules to magnetic resonance spectra: experts' consensus recommendations. *NMR Biomed*. In press
84. Near J. Spectral quantification and pitfalls in interpreting MRS data—what to look out for. In: Rothman DL, Stagg C, eds. *Magnetic Resonance Spectroscopy: Tools for Neuroscience Research and Emerging Clinical Applications*. Amsterdam, The Netherlands: Elsevier; 2014:49-67.
85. Barantin L, Le Pape A, Akoka S. A new method for absolute quantitation of MRS metabolites. *Magn Reson Med*. 1997;38:179-182.
86. Thulborn KR, Ackerman JJH. Absolute molar concentrations by NMR in inhomogeneous B_1. A scheme for analysis of *in vivo* metabolites. *J Magn Reson*. 1983;55:357-371.
87. Kreis R, Ernst T, Ross BD. Absolute quantitation of water and metabolites in the human brain. II. Metabolite concentrations. *J Magn Reson B*. 1993;102:9-19.
88. Christiansen P, Henriksen O, Stubgaard M, Gideon P, Larsson HB. In vivo quantification of brain metabolites by ^{1}H-MRS using water as an internal standard. *Magn Reson Imaging*. 1993;11:107-118.
89. Barker PB, Soher BJ, Blackband SJ, Chatham JC, Mathews VP, Bryan RN. Quantitation of proton NMR spectra of the human brain using tissue water as an internal concentration reference. *NMR Biomed*. 1993;6:89-94.
90. Gasparovic C, Song T, Devier D, et al. Use of tissue water as a concentration reference for proton spectroscopic imaging. *Magn Reson Med*. 2006;55:1219-1226.
91. Alger JR. Quantitative proton magnetic resonance spectroscopy and spectroscopic imaging of the brain: a didactic review. *Topics Magn Reson Imaging*. 2010;21:115-128.
92. Gasparovic C, Neeb H, Feis DL, et al. Quantitative spectroscopic imaging with in situ measurements of tissue water T_1, T_2, and density. *Magn Reson Med*. 2009;62:583-590.

93. MacKay A, Whittall K, Adler J, Li D, Paty D, Graeb D. In vivo visualization of myelin water in brain by magnetic resonance. *Magn Reson Med*. 1994; 31:673-677.
94. Nagae-Poetscher LM, McMahon M, Braverman N, et al. Metabolites in ventricular cerebrospinal fluid detected by proton magnetic resonance spectroscopic imaging. *J Magn Reson Imaging*. 2004;20:496-500.
95. Leen WG, Willemsen MA, Wevers RA, Verbeek MM. Cerebrospinal fluid glucose and lactate: age-specific reference values and implications for clinical practice. *PloS ONE*. 2012;7:e42745.
96. Hourani BT, Hamlin EM, Reynolds TB. Cerebrospinal fluid glutamine as a measure of hepatic encephalopathy. *Arch Intern Med*. 1971;127:1033-1036.
97. Madeira C, Vargas-Lopes C, Brandao CO, et al. Elevated glutamate and glutamine levels in the cerebrospinal fluid of patients with probable Alzheimer's disease and depression. *Front Psych*. 2018;9:561.
98. Lin MS. Measurement of spin-lattice relaxation times in double spin-echo imaging. *Magn Reson Med*. 1984;1:361-369.
99. Kreis R. Quantitative localized ^{1}H MR spectroscopy for clinical use. *Prog Nucl Magn Reson Spectrosc*. 1997;31:155-195.
100. Gasparovic C, Chen H, Mullins PG. Errors in ^{1}H-MRS estimates of brain metabolite concentrations caused by failing to take into account tissue-specific signal relaxation. *NMR Biomed*. 2018;31:e3914.
101. Gussew A, Erdtel M, Hiepe P, Rzanny R, Reichenbach JR. Absolute quantitation of brain metabolites with respect to heterogeneous tissue compositions in ^{1}H-MR spectroscopic volumes. *Magn Reson Mater Phys Biol Med*. 2012;25:321-333.
102. Kirov II, Fleysher L, Fleysher R, Patil V, Liu S, Gonen O. Age dependence of regional proton metabolites T_2 relaxation times in the human brain at 3 T. *Magn Reson Med*. 2008;60:790-795.
103. Marjanska M, Emir UE, Deelchand DK, Terpstra M. Faster metabolite ^{1}H transverse relaxation in the elder human brain. *PloS ONE*. 2013;8:e77572.
104. Jiru F, Skoch A, Wagnerova D, et al. The age dependence of T_2 relaxation times of N-acetyl aspartate, creatine and choline in the human brain at 3 and 4T. *NMR Biomed*. 2016;29:284-292.
105. Rooney WD, Johnson G, Li X, et al. Magnetic field and tissue dependencies of human brain longitudinal $^{1}H_2O$ relaxation in vivo. *Magn Reson Med*. 2007;57:308-318.
106. Vymazal J, Righini A, Brooks RA, et al. T1 and T2 in the brain of healthy subjects, patients with Parkinson disease, and patients with multiple system atrophy: relation to iron content. *Radiology*. 1999;211:489-495.
107. McIntyre DJ, Charlton RA, Markus HS, Howe FA. Long and short echo time proton magnetic resonance spectroscopic imaging of the healthy aging brain. *J Magn Reson Imaging*. 2007;26:1596-1606.
108. Chiu PW, Mak HK, Yau KK, Chan Q, Chang RC, Chu LW. Metabolic changes in the anterior and posterior cingulate cortices of the normal aging brain: proton magnetic resonance spectroscopy study at 3 T. *Age*. 2014;36:251-264.
109. Eylers VV, Maudsley AA, Bronzlik P, Dellani PR, Lanfermann H, Ding XQ. Detection of normal aging effects on human brain metabolite concentrations and microstructure with whole-brain MR spectroscopic imaging and quantitative MR imaging. *Am J Neuroradiol*. 2016;37:447-454.
110. Inglese M, Li BS, Rusinek H, Babb JS, Grossman RI, Gonen O. Diffusely elevated cerebral choline and creatine in relapsing-remitting multiple sclerosis. *Magn Reson Med*. 2003;50:190-195.
111. Vrenken H, Barkhof F, Uitdehaag BM, Castelijns JA, Polman CH, Pouwels PJ. MR spectroscopic evidence for glial increase but not for neuro-axonal damage in MS normal-appearing white matter. *Magn Reson Med*. 2005;53:256-266.
112. Gasparovic C, Prestopnik J, Thompson J, et al. ^{1}H-MR spectroscopy metabolite levels correlate with executive function in vascular cognitive impairment. *J Neurol Neurosurg Psychiatry*. 2013;84:715-721.
113. Rackayova V, Cudalbu C, Pouwels PJW, Braissant O. Creatine in the central nervous system: from magnetic resonance spectroscopy to creatine deficiencies. *Anal Biochem*. 2017;529:144-157.
114. Michaelis T, Merboldt KD, Bruhn H, Hanicke W, Frahm J. Absolute concentrations of metabolites in the adult human brain in vivo: quantification of localized proton MR spectra. *Radiology*. 1993;187:219-227.
115. Helms G. A precise and user-independent quantification technique for regional comparison of single volume proton MR spectroscopy of the human brain. *NMR Biomed*. 2000;13:398-406.
116. Heinzer-Schweizer S, De Zanche N, Pavan M, et al. *In-vivo* assessment of tissue metabolite levels using 1H MRS and the electric REference to access in vivo concentrations (ERETIC) method. *NMR Biomed*. 2010;23:406-413.
117. Zoelch N, Hock A, Heinzer-Schweizer S, Avdievitch N, Henning A. Accurate determination of brain metabolite concentrations using ERETIC as external reference. *NMR Biomed*. 2017;30:e3731.
118. Desal H, Pineda Alonso N, Akoka S. Electronic reference for absolute quantification of brain metabolites by ^{1}H-MRS on clinical whole-body imaging. *J Neuroradiol*. 2010;37:292-297.
119. Frahm J, Merboldt K-D, Hänicke W. Localized proton spectroscopy using stimulated echoes. *J Magn Reson*. 1987;72:502-508.

SUPPORTING INFORMATION

Additional supporting information may be found online in the Supporting Information section at the end of this article.

How to cite this article: Near J, Harris AD, Juchem C, et al. Preprocessing, analysis and quantification in single-voxel magnetic resonance spectroscopy: experts' consensus recommendations. *NMR in Biomedicine*. 2021;34:e4257. https://doi.org/10.1002/nbm.4257